DESIGN AND DEVELOPMENT OF A SELF-BALANCING BICYCLE USING CONTROL MOMENT GYRO

Pom Yuan Lam

(B.Eng. (Hons.), NTU)

A THESIS SUBMITTED

FOR THE DEGREE OF MASTER OF ENGINEERING

DEPARTMENT OF MECHANICAL ENGINEERING

NATIONAL UNIVERSITY OF SINGAPORE

2012

DECLARATION

I hereby declare that the thesis is my original work and it had been written by me in its entirety.

I have duly acknowledged all the sources of information which have been used in the thesis.

This thesis has also not been submitted in any university previously.

Pom Yuan Lam

4 March 2013

ACKNOWLEDGMENTS

The author wishes to express his heart-felt gratitude to his supervisor, Associate Professor Marcelo H. Ang Jr for his guidance through the years. He is grateful to Professor Ang for providing him with a lot of opportunities to extend his knowledge and to develop his skills.

SUMMARY

Bicycles provide transportation for leisure, recreation, and travel between home and work, throughout the world, in big cities as well as in small villages, supporting human mobility for more than a century. This widespread vehicle is the least expensive means of wheeled transportation.

The bicycle was continually developed during the last quarter of the 19th century and the 20th century, leading to the high-performance modern wheeled transportation of today. An account of bicycle evolution can be found in [1] as well as in the Proceedings of the International Cycling History Conference, held every year since 1990 [2].

Modelling, analysis and control of bicycle dynamics has been an attractive area of research. Bicycle dynamics has attracted the attention of the automatic control research community due to its non-intuitive nature, for example, the fact that it depends strongly on the bicycle speed. The bicycle displays interesting dynamics behaviour. It is statically unstable like the inverted pendulum, but under certain conditions, is stable in forward motion [3]. Under some conditions, it exhibits both open-loop right-half plane poles and zeros [4], making the design of feedback controllers for balancing in the upright position or moving along a predefined path a challenging problem.

This work uses a control moment gyro (CMG) as an actuator. The control moment gyro (CMG) is typically used in a spacecraft to orient the vessel [5]. Appling a CMG as an actuator to balance a bicycle is a creative and novel approach; and is the first of its kind for balancing of a bicycle. Simulation exercises showed that a PD controller is adequate to for balancing the bicycle. A real-time controller was implemented on a kid-

size bicycle and the bicycle was successfully balanced and able to move forward, reversing and small angle turning. Further research such as adaptive control can be added to the system so that the system can react to changes in payload.

TABLE OF CONTENTS

Contents

LIST OF FIGURES

LIST OF TABLES

NOMENCLATURE

m_f	Mass of flywheel
m_b	Mass of bicycle
h_f	Flywheel c.g. upright height
h_b	Bicycle c.g. upright height
I_b	Bicycle moment of inertia around ground contact line
I_p	Flywheel polar moment of inertia around c.g.
I_r	Flywheel radial moment of inertia around c.g.
ω	Flywheel angular velocity
L	Motor Inductance
R	Motor Resistance
B_m	Motor viscosity coefficient
K_m	Motor torque constant
K_e	Motor back emf constant
g	Gravitational acceleration

Chapter 1. INTRODUCTION

1.1 Background

The bicycle's environmental friendliness and light weight make it a good means of transportation. A robot bicycle is, by nature, an unstable system whose inherent nonlinearity makes it difficult to control. This in turn, brings interesting challenges to the control engineering community. Researchers have been exploring different mechatronic solutions for dynamically balancing and manoeuvring robot bicycles [6].

A self-balancing robot bicycle uses sensors to detect the roll angle of the bicycle and actuators to bring it into balance as needed, similar to an inverted pendulum. It is thus an unstable nonlinear system.

A self-balancing robot bicycle can be implemented in several ways. In this work, we review these methods, and introduce our mechanism which involves a control moment gyro (CMG); -- an attitude control device typically used in spacecraft attitude control systems [6]. A CMG consists of a spinning rotor and one or more motorized gimbals that tilt the rotor's angular momentum. As the rotor tilts, the changing angular momentum causes gyroscopic precession torque that balances the bicycle.

A bicycle is inherently unstable and without appropriate control, it is uncontrollable and cannot be balanced. There are several different methods for

balancing of robot bicycles, such as the use of gyroscopic stabilization by Beznos et al. in 1998 [8]. The stabilisation unit consist of two coupled gyroscopes spinning in opposite directions. It makes use of the gyroscopic torque due to the precession of gyroscopes. This torque counteracts the destabilising torque due to gravity forces.

Lee and Ham in 2002 [9] proposed a load mass balance system. A control strategy was developed to turn the bicycle system left or right by moving the centre of a load mass left and right respectively.

Tanaka and Murakami in 2004 [10] proposed the use of steering control to balance the bicycle. The control method for bicycle steering based on acceleration control is proposed. The steer angle was controlled via a servo motor, and an electric motor was used to maintain forward speed. The dynamic model for the bicycle is derived from equilibrium of gravity and centrifugal force. The bicycle was tested on a treadmill apparatus and the controller demonstrated the ability to stabilise the bicycle effectively.

A very well-known self-balancing robot bicycle, Murata Boy, was developed by Murata in 2005 [11]. Murata Boy (Figure 1.1) uses a reaction wheel inside the robot as a torque generator, as an actuator to balance the bicycle. The reaction wheel consists of a spinning rotor, whose spin rate is nominally zero. Its spin axis is fixed to the bicycle, and its speed is increased or decreased to generate reaction torque around the spin axis. Reaction wheels are the simplest and least expensive of all momentum-exchange actuators. Its advantages are low cost, simplicity, and the absence of ground

reaction. Its disadvantages are that it consumes more energy and cannot produce large amounts of torque.

Figure 1.1: Murata Boy [10], self-balancing riding robot.

In another approach proposed by Gallaspy [12], the bicycle can be balanced by controlling the torque exerted on the steering handlebar. Based on the amount of roll, a controller controls the amount of torque applied to the handlebar to balance the bicycle. Advantages of such a system include low mass and low energy consumption. Disadvantages of such as system is its lack of robustness against large roll disturbance.

Among these methods, the CMG, a gyroscopic stabilizer is a good choice because its response time is short [13] and the system is stable when the bicycle is stationary. The CMG consists of a spinning rotor with a large, constant angular momentum, whose angular momentum vector direction can be changed for a bicycle by rotating the spinning rotor. The spinning rotor, which is on a gimbal, applies a torque to the gimbal to produce a precessional, gyroscopic reaction torque orthogonal to both the rotor spin and gimbal axes. A CMG amplifies torque because a small gimbal torque input produces a large control torque [14] to the bicycle. CMG had been typically used in spacecraft to orient the vessel, Figure 1.2 shows a Pleiades spacecraft that uses three CMG to provide a roll, yaw and pitch actuation.

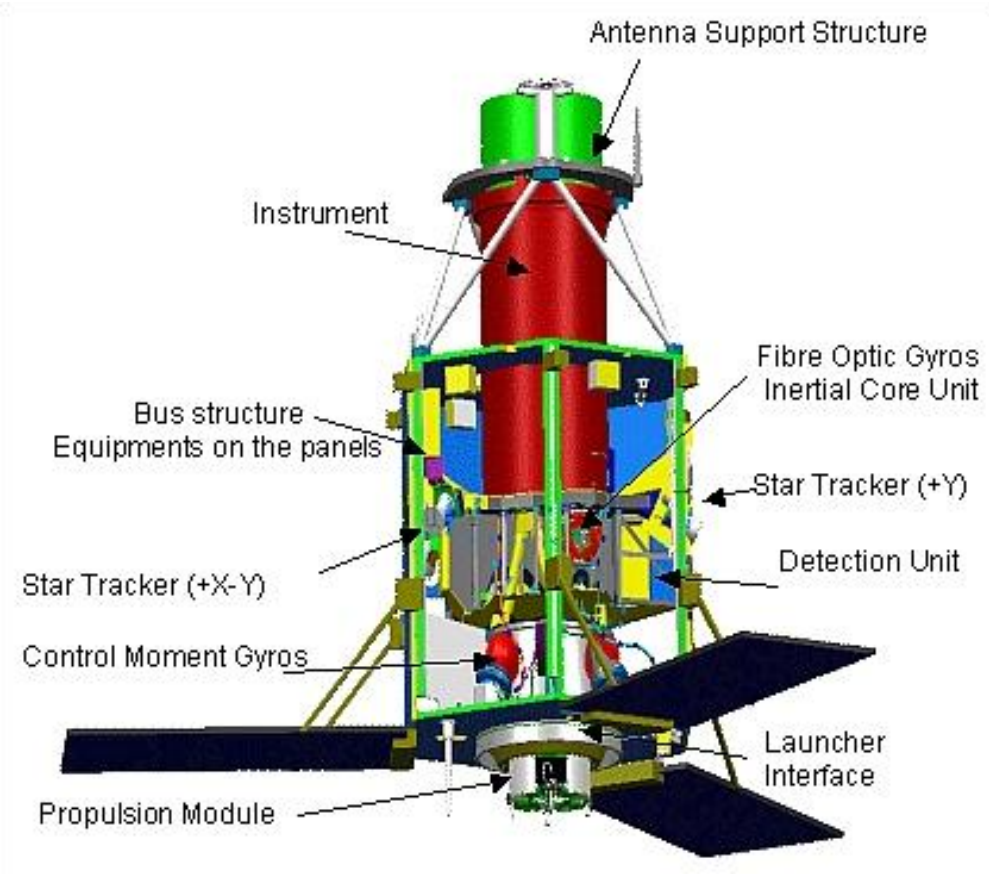

Figure 1.2: CMG used in Pleiades spacecraft [7].

The robot described in this work uses the CMG as a momentum exchange actuator to balance the bicycle. Advantages of such a system include its being able to produce large amounts of torque and having no ground reaction force. The CMG has not been widely used as an actuator other than on large spacecraft to control the attitude of large spacecraft and space infrastructure such as the International Space Station [15]. There are many reasons for this, but mainly this is due to the complexity of the mechanical and control system needed to implement an effective CMG, and also because off-the-shelf CMG systems are generally made for larger satellite market. Large torque amplification and momentum storage capacity are two basic properties that make CMG superior when compared to the reaction wheels. Compared with reaction wheels, CMG are relatively lightweight and they have a capability to generate higher torque levels per unit kg [15].

1.2 Objectives

The objective of this work is to investigate and implement a control algorithm on a sbRIO (Single Board Reconfigurable IO) to control a CMG (Control Moment Gyro) which in turn generates a precessional torque to balance a bicycle.

1.3 Scope of Work

The scope of work includes the following:

1) Modelling of the dynamics of the bicycle.
2) Design and simulate a suitable controller.

3) Interface an IMU (Inertial Moment Sensing Unit) to sbRIO to measure roll the angle of the bicycle.
4) Implement a real-time controller in sbRIO to balance a real bicycle

1.4 Contribution of this Thesis

This thesis provides a comparison of the various methods to balance a bicycle, evaluated their advantages and disadvantages. The most significant contribution of this research is the use of a CMG as an actuator to balance the bicycle. By making use of the principle of gyroscopic precession, a novel methodology was developed to harness the gyroscopic precessional torque to balance the bicycle.

1.5 Thesis Outline

The outline of the thesis is as follows:

Chapter 2 This chapter derives a simplified dynamical model of the CMG-Controlled Bicycle and how it achieves self-balancing. Computer simulations were conducted to determine the stability of the un-compensated and compensated-for system.

Chapter 3 This chapter describes the various subsystems of the mechatronics system and encoder noise issue and how it was resolved.

Chapter 4 This chapter reports on experimental data on the self-balancing bicycle and explains how the bicycle achieves basic motion of moving forward and turning.

Chapter 5 This chapter gives the conclusion of the work, some achievements and awards that this project had won. Some possible future works are also discussed in this chapter.

Chapter 2. BASIC CONCEPTS

2.1 Dynamic Model of CMG-Controlled Bicycle

A control momentum gyroscope (CMG) is an attitude control device that is generally used in spacecraft attitude control systems. It consists of a spinning rotor and one or more motorized gimbals that tilt the rotor's angular momentum. As the rotor tilts, the changing angular momentum causes a gyroscopic torque that rotates the spacecraft.

This project employs a single axis CMG which is the most energy-efficient among different design of CMGs. As the motorised gimbal of a single axis CMG rotates, the change in direction of the rotor's angular momentum generates a precessional torque that reacts onto the frame of the bicycle to which the CMG is mounted. The precessional torque generated is used to balance the bicycle. Single-gimbal CMG exchange angular momentum is very efficient and requires very little power. Large amount of torque can be generated for relatively small electrical input to the gimbal motor; CMG is a torque amplification device. The bicycle relies on gyroscopic precession torque to stabilize the bicycle while it is upright. Figure 2.1 shows how precession torque balances the bicycle.

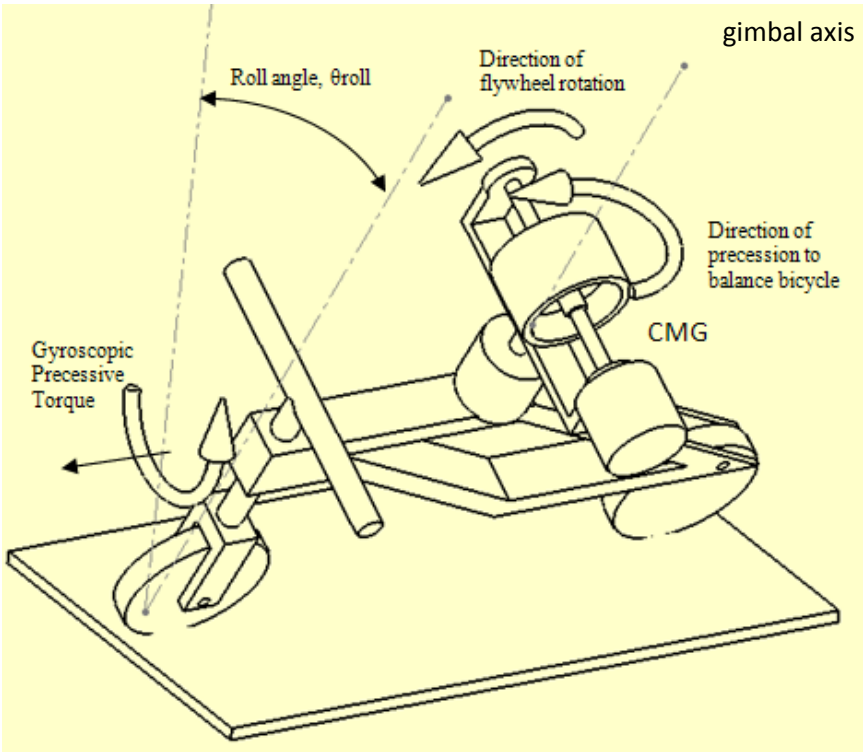

Figure 2.1: Balancing of bicycle using gyroscopic precession torque generated by CMG.

When the bicycle is tilted at angle θ_{roll} as shown in Figure 2.1, an inertia measurement unit (IMU) sensor detects the roll angle. Roll data is fed to an on-board controller that in turn commands the CMG's gimbal motor to rotate so that gyroscopic precession torque is produced to balance the bicycle upright. The system uses a single gimbal CMG and generates only one axis torque. The direction of output torque change is based on gimbal motion. Figure 2.2 shows the components and vectors of a single gimbal CMG. The system uses gyroscopic torque to balance the bicycle. With reference to Figure 2.1, when the CMG precess about the gimbal axis, a gyroscopic torque normal to the frame of the bicycle will be generated to balance the bicycle. [15] is a short video to illustrate how the CMG attempts to balance a bicycle.

The amount of toque produced depends on angular momentum of the flywheel. Hence, in order to generate the highest possible gyroscopic precessive torque; the flywheel motor will be running at its maximum possible speed of 4480 rpm.

The flywheel angular nominal speed is 4480 rpm, so ω is 469 rad/s. To analyse the amount of torque that the CMG could generate, a flywheel was designed in Computer Aided Design (CAD) software and to be made of brass; due to its high density. The flywheel designed polar moment of inertia ($I_{p)}$ is 0.0088 kg.m^2.

Angular momentum of rotor, $Z = I_p\omega_{fly}$

$= 0.00883 \times 469$

$= 4.14$ kg-m^2/s

If a rotational precession rate of ω_D, is applied to the spinning flywheel around the gimbal axis, precession output torque T, which is perpendicular to the direction of ω_{fly}, and ω_D is generated as shown in Figure 2.2. The angular velocity of gimbal can be set at an arbitrary number within the nominal output of the motor. The faster the angular velocity the higher the generated torque. For example, we set an angular velocity of 5 rad/s, so the gimbal precession output torque generated is:

$T_p = Z\omega_D$

$= 4.14 \times 5$

$= 20.7$ Nm

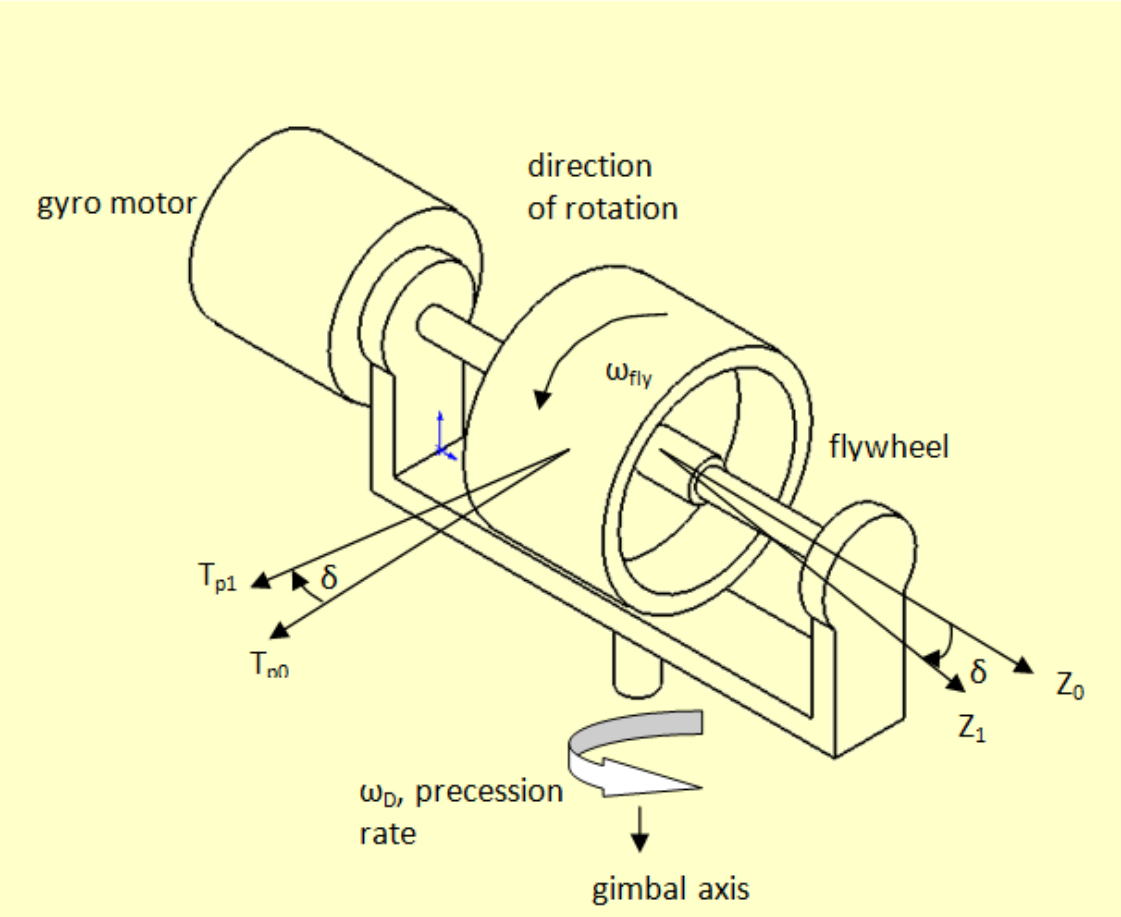

Figure 2.2: Components of a single-axis CMG.

The dynamic model of a bicycle is based on the equilibrium of gravity and centrifugal force. A simplified model for balancing is derived using the Lagrange method and neglecting force generated by the bicycle moving forward and steering. This model is based on the work of Parnichkun[17], which is a simplified dynamics model of the bicycle for balancing control while derived using the Lagrange method and neglecting force generated, as stated, by the bicycle moving forward and steering. With reference to Figure 2.3, the system, consisting of two rigid body links, has as its first link a bicycle frame having 1 degree-of-freedom (DOF) rotation around the Z axis. The second link is the flywheel, which is assumed to have constant speed ω. The flywheel centre of gravity (COG) is fixed relative to the bicycle frame.

When the flywheel rotates at a constant speed around X1 axis and we control the angular position of the gimbal axis around the Y1 axis, angular momentum on the Z1 axis generates a torque, called precession torque (in the direction of Z1 axis), through a gyroscopic effect, and is used to balance the bicycle.

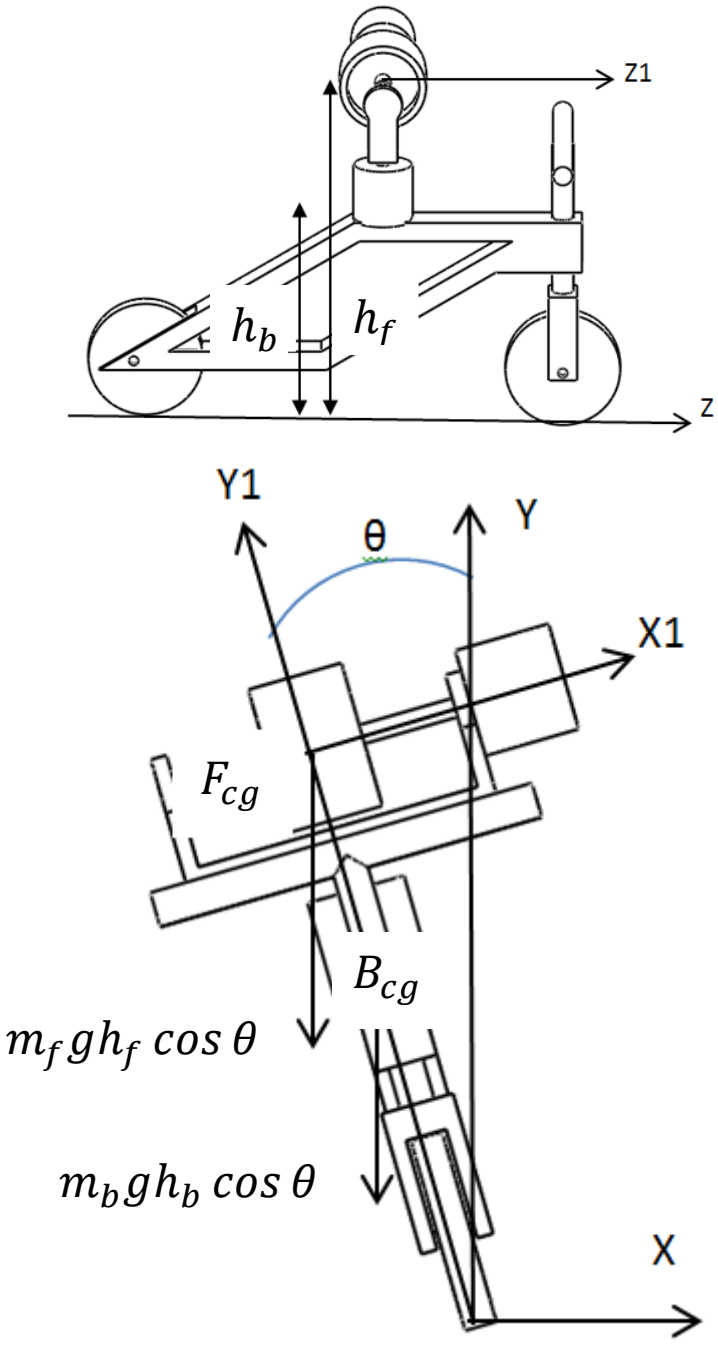

Figure 2.3: Reference coordinates of bicycle.

In Figure 2.3, Bcg and Fcg denotes bicycle and flywheel COG. The roll angle around the Z axis is defined by θ, and the angular position of the gimbal axis of the flywheel with respect to Y1 axis is as shown in Figure 4. The angular velocity of the bicycle about the Z axis is defined as $\dot{\theta}$ and the angular velocity of the flywheel about its gimbal axis is defined as $\dot{\delta}$. Since the flywheel COG does not move relative to the bicycle COG, absolute velocities of B_{cg} and F_{cg} are:

$$|V_b| = \dot{\theta} h_B \tag{2.1}$$

$$|V_f| = \dot{\theta} h_f \tag{2.2}$$

where h_B is the height of the bicycle COG in relation to the ground and h_f is the height of the COG of its flywheel counterpart. A Lagrange equation [6] is used to derive the dynamic model of the system:

$$\frac{d}{dt}\left\{\frac{\partial T}{\partial q_i}\right\} - \frac{\partial T}{\partial q_i} + \frac{\partial V}{\partial q_i} = Q_i \tag{2.3}$$

where T is total system kinetic energy, V is total system potential, Q_i is external force, and q_i is a generalized coordinate. V and T are determined, represented as follows:

$$V = m_b g h_b \cos\theta + m_f g h_f \cos\theta \tag{2.4}$$

$$T = \frac{1}{2}m_b(|v_b|)^2 + \frac{1}{2}m_f\left(|v_f|\right)^2 + \frac{1}{2}I_b\dot{\theta}^2 + \frac{1}{2}\left[I_r\dot{\delta}^2 + I_p\left(\dot{\theta}\sin\delta\right)^2 + I_r\left(\dot{\theta}\cos\delta\right)^2\right]$$

$$T = \frac{1}{2}m_b\left(\dot{\theta}^2{h_b}^2\right) + \frac{1}{2}m_f\left(\dot{\theta}^2{h_f}^2\right) + \frac{1}{2}I_b\dot{\theta}^2 + \frac{1}{2}\left[I_r\dot{\delta}^2 + I_p\left(\dot{\theta}\,sin\,\delta\right)^2 + I_r\left(\dot{\theta}\,cos\,\delta\right)^2\right] \tag{2.5}$$

where I_p is the flywheel polar moment of inertia around c.g. and I_r is the flywheel radial moment of inertia around c.g., m_b is the mass of the bicycle, and m_f is the mass of the flywheel. I_b is the bicycle moment of inertia around ground contact line.

For $q_i = \theta$, the Lagrange equation becomes

$$\frac{d}{dt}\left\{\frac{\partial T}{\partial\dot{\theta}}\right\} - \frac{\partial T}{\partial\theta} + \frac{\partial V}{\partial\theta} = Q_\theta \tag{2.6}$$

Using Equations (2.4) - (2.6), we have

$$\ddot{\theta}\left[m_b h_b^2 + m_f h_f^2 + I_b + I_p sin^2\delta + I_r cos^2\delta\right] + 2sin\delta cos\delta\left(I_p - I_r\right)\dot{\theta}\dot{\delta} - g\left(m_b h_b + m_f h_f\right)sin\theta = I_p\omega\dot{\delta}cos\delta \tag{2.7}$$

For $q_i = \delta$, the Lagrange equation becomes

$$\frac{d}{dt}\left\{\frac{\partial T}{\partial \dot{\delta}}\right\} - \frac{\partial T}{\partial \delta} + \frac{\partial V}{\partial \delta} = Q_\delta \tag{2.8}$$

Using Equations (2.4), (2.5), and (2.8) yields the following equation:

$$\ddot{\delta} I_r - \dot{\theta}^2 \left(I_p - I_r\right) sin\delta cos\delta = T_m - I_p \omega \dot{\theta} cos\delta - B_m \dot{\delta} \tag{2.9}$$

where B_m is the DC motor viscosity coefficient. The DC motor is coupled to the gimbal of the Flywheel via a final 65:1 ratio combining a planetary gear head and belt-drive.

$$T_m = 65 K_m i \tag{2.10}$$

$$U = L\frac{di}{dt} + R_i + K_e \dot{\delta} \tag{2.11}$$

where K_m, K_e are torque and back EMF constants of the motor. R_i and L are resistance and inductance of the motor. T_m is torque generated by the motor and U is voltage applied to the motor.

The summary of the equations of the dynamic model of the bicycle is as follows:

$$\text{Input} = U = L\frac{di}{dt} + R_i + K_e\dot{\delta}$$

Output = rate of precession of the CMG =

$$\ddot{\delta} = \frac{T_m - I_p\omega\dot{\theta}cos\delta - B_m\dot{\delta} + \dot{\theta}^2(I_p - I_r)sin\delta cos\delta}{I_r}$$

These dynamics focuses only on the balancing of the bicycle. The other inputs to allow the translation of the bicycle are independent of these dynamics. Whatever these translational motions are, the CMG will maintain balance at all times as long as steering is not changed so much nor abruptly.

2.2 Bicycle Self-Balancing

Equations (2.7) – (2.9) model the dynamics of the bicycle. Equations (2.10) to (2.11) relate the torque generated with the voltage applied to the motor and represent the dynamics of the electrical system.

Linearization allows easy application of classical control theory to develop practical algorithms that can be implemented in real-time. The bicycle is also meant to operate at a limited balancing range that does not change so much to maintain the bicycle at its upright (equilibrium) position.

By substitution of equation (2.10) into equation (2.9), and linearization of the equation (2.7) and equation (2.9) around the equilibrium position ($\theta = \delta = 0$) yields:

$$\ddot{\theta}\left[m_b h_b^2 + m_f h_f^2 + I_b + I_r\right] - g\left(m_b h_b + m_f h_f\right)\theta - I_p \omega \dot{\delta} = 0 \tag{2.12}$$

$$\ddot{\delta} I_r - I_p \omega \dot{\theta} + B_m \dot{\delta} - 65 K_m i = 0 \tag{2.13}$$

Define $= \begin{bmatrix} \theta \\ \dot{\theta} \\ \delta \\ \dot{\delta} \end{bmatrix}$, $y = \theta$ and $u = U$. The dynamics model of the system in state-space representation by combining (2.11), (2.12), and (2.13) is shown by the following equation:

$$\dot{x} = Ax + Bu \tag{2.14}$$

$$y = Cx + Du \tag{2.15}$$

where

$$A = \begin{bmatrix} 0 & 1 & 0 & 0 \\ \dfrac{g(m_b h_b + m_f h_f)}{m_b h_b^2 + m_f h_f^2 + I_b + I_r} & 0 & \dfrac{I_p \omega}{m_b h_b^2 + m_f h_f^2 + I_b + I_r} & 0 \\ 0 & -\dfrac{I_p \omega}{I_r} & -\dfrac{B_m}{I_r} & \dfrac{65 K_m}{I_r} \\ 0 & 0 & -\dfrac{K_e}{L} & -\dfrac{R}{L} \end{bmatrix}$$

$$B = \begin{bmatrix} 0 \\ 0 \\ 0 \\ \frac{1}{L} \end{bmatrix}, \quad C = \begin{bmatrix} 1 & 0 & 0 & 0 \end{bmatrix}, \text{ and } D = [0] \tag{2.16}$$

We have built a CMG-balance bicycle robot with parameters listed in Table 1. The bicycle was a kid-size bicycle purchased off-the-shelf, with a mass of 20.6 kg. Dimension of the flywheel is designed such that it was able to generate the required balancing torque. The flywheel motor will be running at its maximum possible speed in order to generate the maximum possible torque, alternatively the flywheel's polar moment of inertia could be increased; but this will also increase the mass of the flywheel; which is undesirable.

Table 2.1: Parameters of self-balancing robot.

Parameters	Value	Unit	Description
m_f	2.02	kg	Mass of flywheel
m_b	20.6	kg	Mass of bicycle
h_f	0.58	m	Flywheel COG upright height
h_b	0.49	m	Bicycle COG upright height
I_b	2.1	$kg.m^2$	Bicycle moment of inertia around ground contact line
I_p	0.0088	$kg.m^2$	Flywheel polar moment of inertia around COG
I_r	0.0224	$kg.m^2$	Flywheel radial moment of inertia around COG
ω	469	rad/s	Flywheel angular velocity
L	0.000119	H	Motor Inductance
R	0.61	Ω	Motor Resistance
B_m	0.003	$kg.m^2/s$	Motor viscosity coefficient
K_m	0.0259	Nm/A	Motor torque constant
K_e	0.0027	V.s	Motor back emf constant
g	9.81	m/s^2	Gravitational acceleration

Using parameters from Table 2.1, system matrices become:

$$A = \begin{bmatrix} 0 & 1 & 0 & 0 \\ 14.26 & 0 & 0.53 & 0 \\ 0 & -184.56 & -0.14 & 75.03 \\ 0 & 0 & -22.69 & -5126 \end{bmatrix}$$

$$B = \begin{bmatrix} 0 \\ 0 \\ 0 \\ 8403 \end{bmatrix}, \quad C = [1 \quad 0 \quad 0 \quad 0], \quad \text{and } D = [0] \tag{2.17}$$

Computing the transfer function from the state variables realization ($\boldsymbol{A}, \boldsymbol{B}, \boldsymbol{C}, \boldsymbol{D}$) yields

$$\frac{\theta(s)}{U(s)} = \frac{334019}{s^4 + 5126.13s^3 + 2470.67s^2 + 428419s - 34040} \tag{2.18}$$

2.3 Computer Simulation

Computer simulation enables the analysis of the system's behaviour without building the hardware. Valuable resources and time can be saved by first modelling and simulating of the system. The bicycle with the CMG is first modelled to determine its stability and subsequently a controller was added to the system to be analysed further for stability.

2.3.1 National Instruments Control Design Assistant (CDA)

The software platform used was the National Instruments control design assistant (CDA). Models can be created from first principle using transfer function, state-space, or zero-pole-gain representation. CDA analyses system performance with tools such as step response, pole-zero maps and Bode plots and allows user to

interactively analyse open and closed-loop behaviour. CDA supports multiple input, multiple output (MIMO) and single input, single output (SISO) systems and take advantage of simulation capabilities to verify linear and nonlinear system dynamics.

2.3.2 Stability Analysis of Uncompensated-For System

With reference to Equation 2.18, a model of the bicycle and CMG or the uncompensated-for system is created in CDA. A Pole-zero analysis was conducted in CDA and results indicate that there are four poles and no zero in the uncompensated-for system. Figure 2.4 shows the pole and zero locations for the uncompensated-for system. There is a pole located on the right half plane which causes the system to be unstable [18].

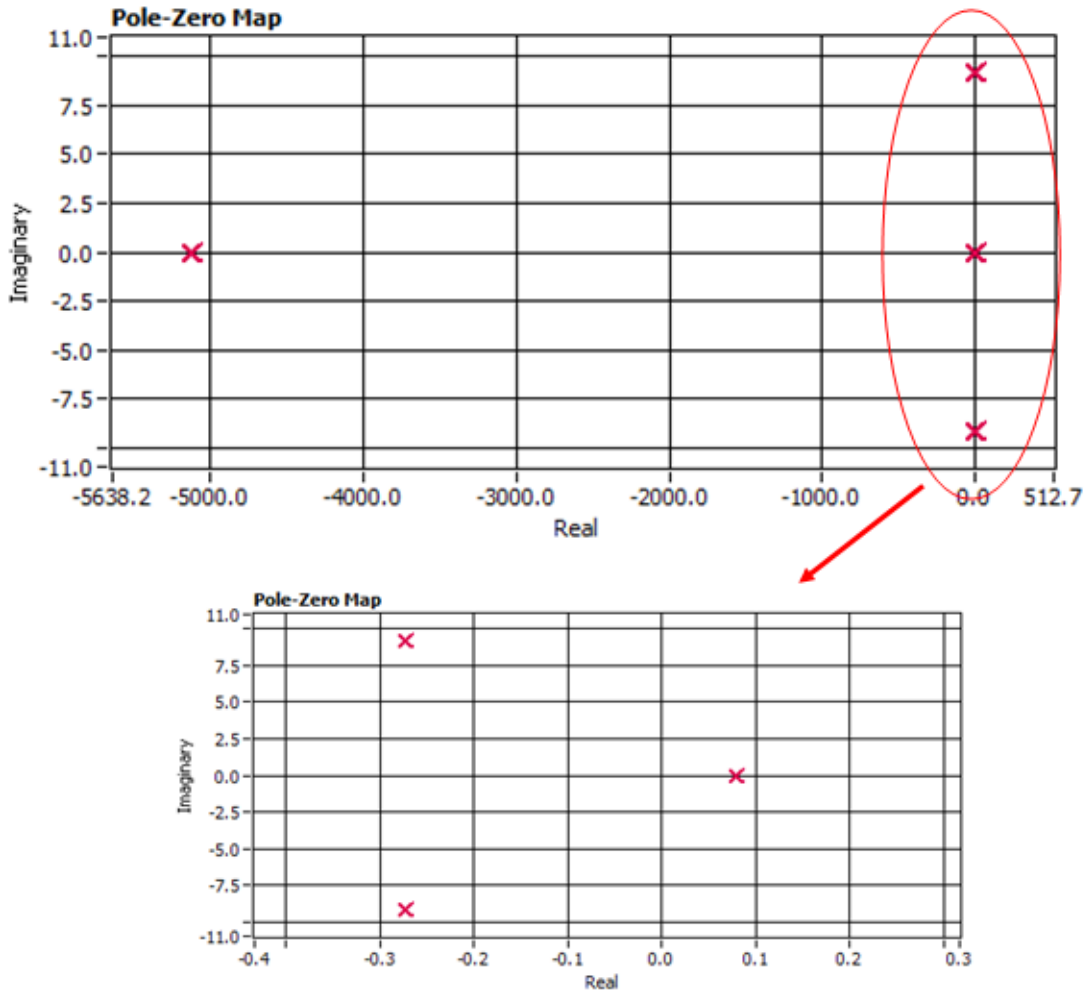

Figure 2.4 : Pole-zero map of uncompensated-for system.

For further stability analysis a Bode plot was done on CDA and Figure 2.5 shows a Bode plot of the uncompensated-for system. Bode plot is a graph of the transfer function of a linear, time-invariant system versus frequency, plotted with a log-frequency axis, for analysis of system's frequency response. It is usually a combination of a Bode magnitude plot, expressing the magnitude of the frequency response gain, and a Bode phase plot, expressing the frequency response phase shift. The phase margin and gain margin must be positive for the system to be stable [19]. From the software, the gain margin was -3.06 and phase margin was -42.97. Negative margins indicate that the system is unstable.

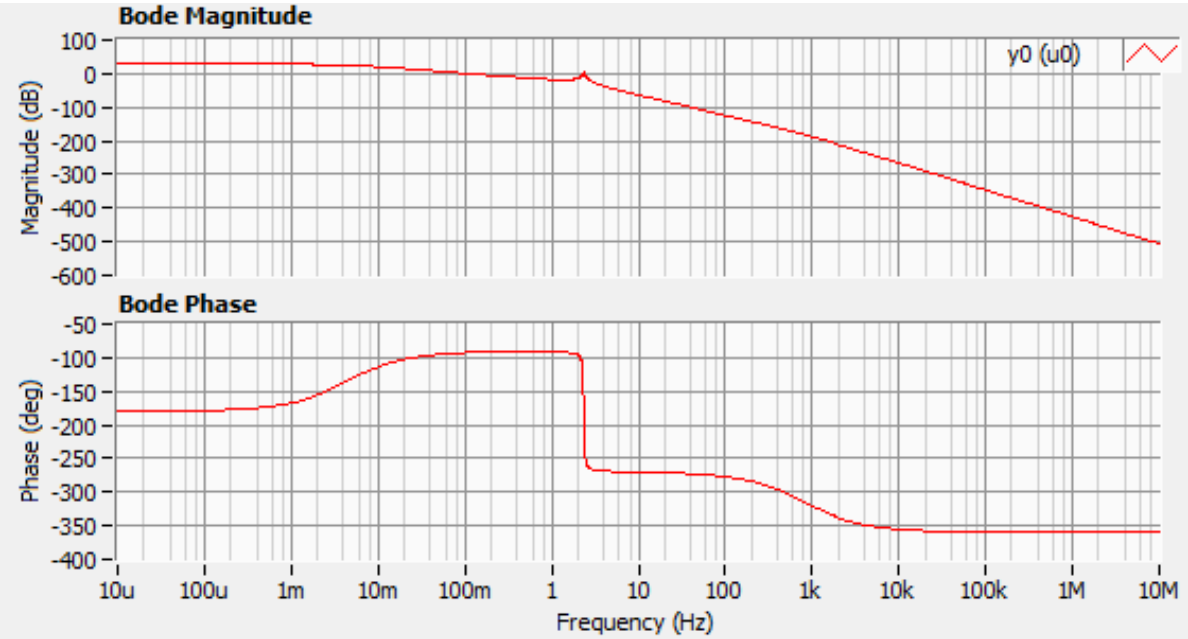

Figure 2.5 : Bode Plot of uncompensated-for system.

2.3.3 Stability Analysis of Proportional plus Derivative (PD) Compensated System

A proportional plus derivative controller was implemented in the CDA as shown in Figure 2.6. Gains were selected by using Ziegler-Nichols rule for tuning [20] and P-Gain was selected to be 25 and D-gain 0.02.

The Ziegler-Nichols tuning method is a heuristic method of tuning a PID controller. It was developed by John G. Ziegler and Nathaniel B. Nichols. It is done by first setting the I (integral) D (derivative) gains to zero. The P (proportional) gain K_p is then increased from zero until it reaches the ultimate gain at which the output oscillates with constant amplitude. The D gain is slowly increased from zero until a suitable step response is achieved.

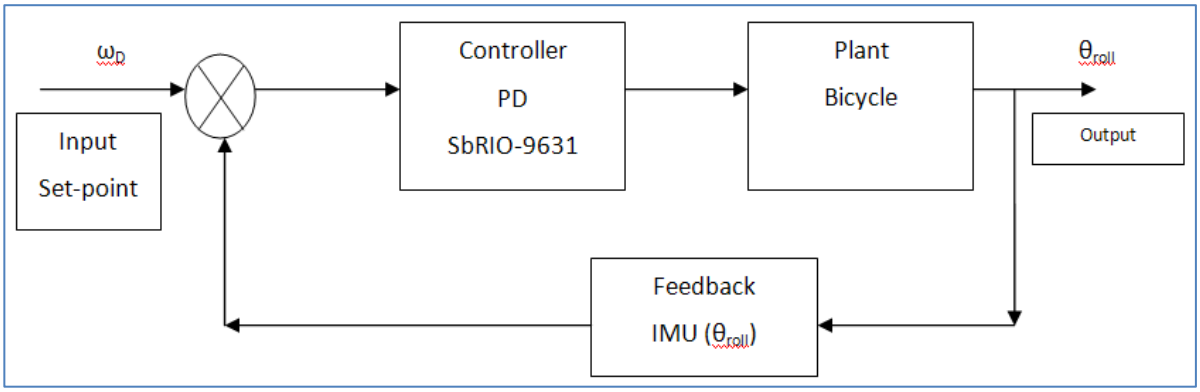

Figure 2.6 : Control block diagram.

Figure 2.7 shows the pole and zero location for the compensated-for system, zeros had been introduced by the controller. The compensated-for system is stable and pole and zero cancellation can clearly be seen in Figure 2.7. The compensated-for system is stable and underdamped.

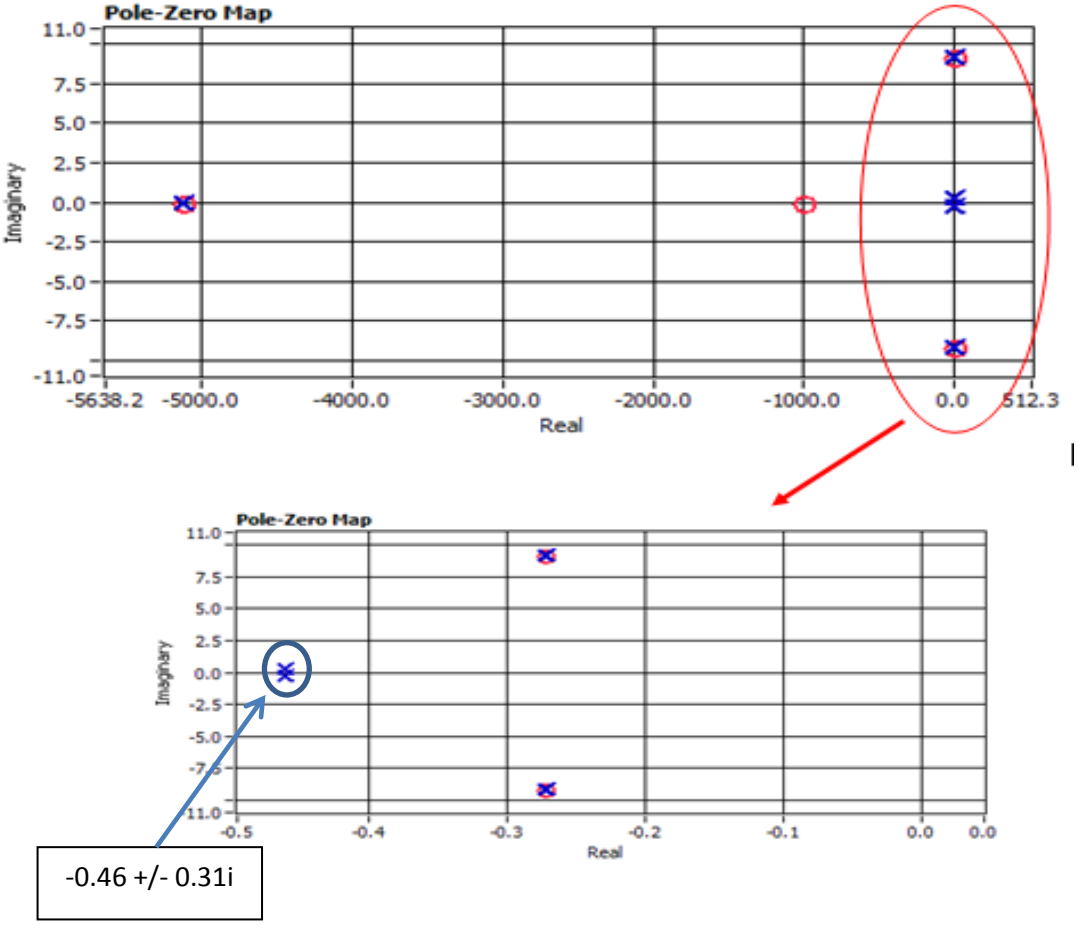

Figure 2.7 : Pole-Zero map of compensated-for system.

Bode Plot was generated for the compensated-for system as shown in Figure 2.8. From the software the gain margin had improved to 6.59 and the phase margin was 86.88. Positive margins indicate that the system is stable.

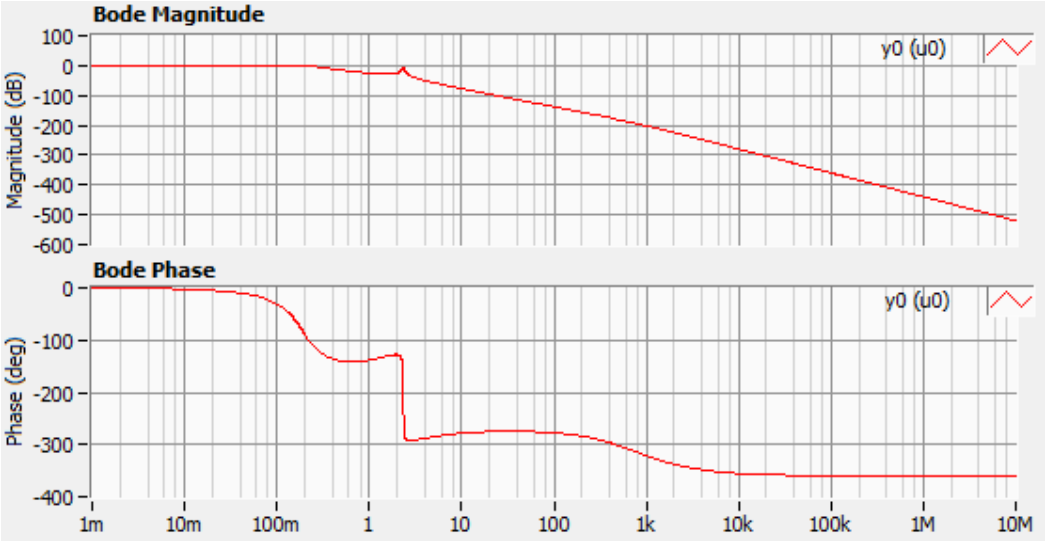

Figure 2.8 : Bode Plot of the compensated-for system.

The effects of increasing the P-Gain was explored using CDA and Figure 2.9 shows the effect of increasing P-Gain from a value of 15 to 35 while keeping the D-Gain constant at 0.02. Clearly, overshoot increases with P-Gain.

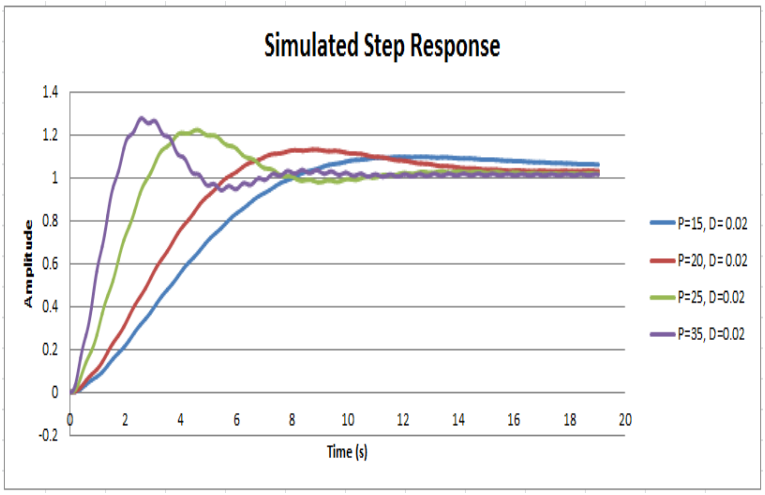

Figure 2.9 : Overshoots increases with increasing P-Gain.

.

2.3.4 Stability Analysis of Proportional-Integral-Derivative (PID) Compensated System

In order to understand the effects of using a PID instead of a PD controller, the PD controller CDA was replaced with a PID controller. Figure 2.10 shows the pole-zero map with the PID controller. The phase margin decreases and a pair of poles had been shifted to the right-half plane. The system becomes unstable and unable to balance the bicycle.

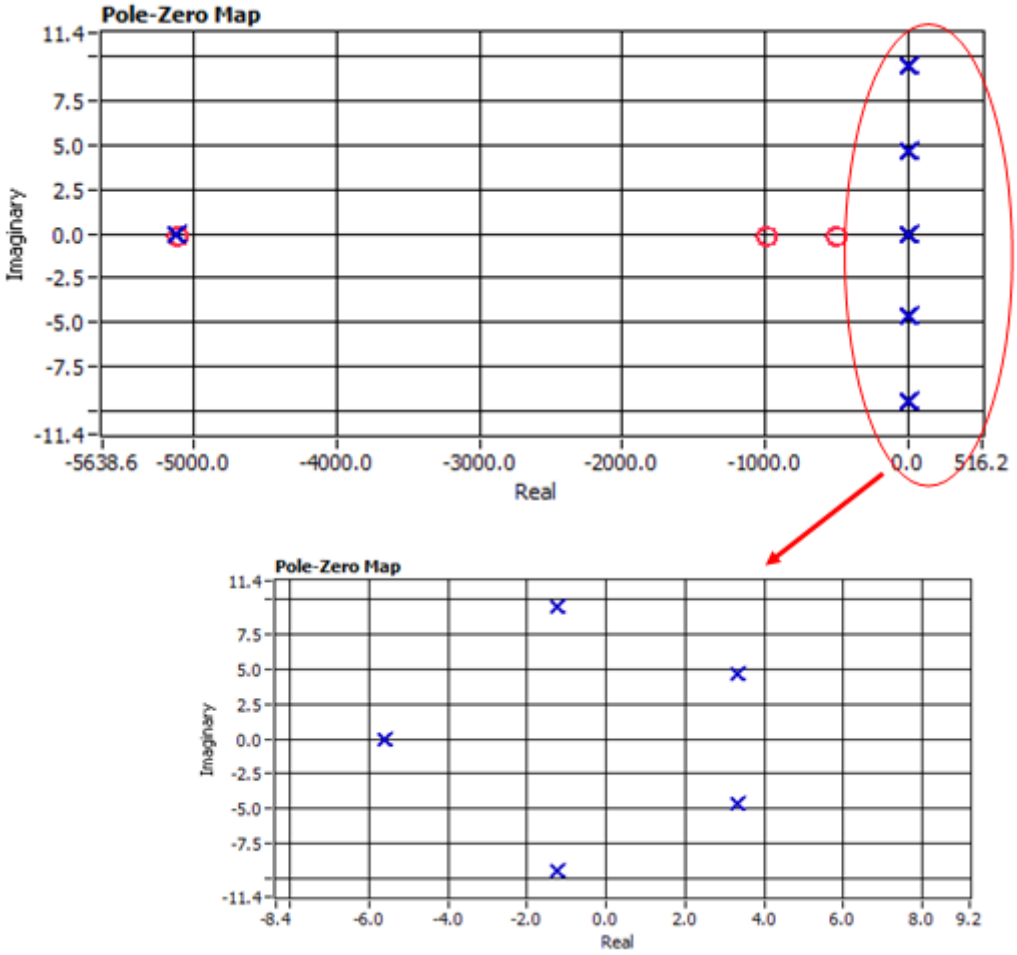

Figure 2.10 : Pole-Zero map of system with PID controller.

Chapter 3. Mechatronic System

3.1 Overview

Figure 3.1 shows the complete mechanical system which consists of an off-the-shelf kid size bicycle and a customized CMG on the bicycle frame. The following section will describe the various mechatronics subsystems.

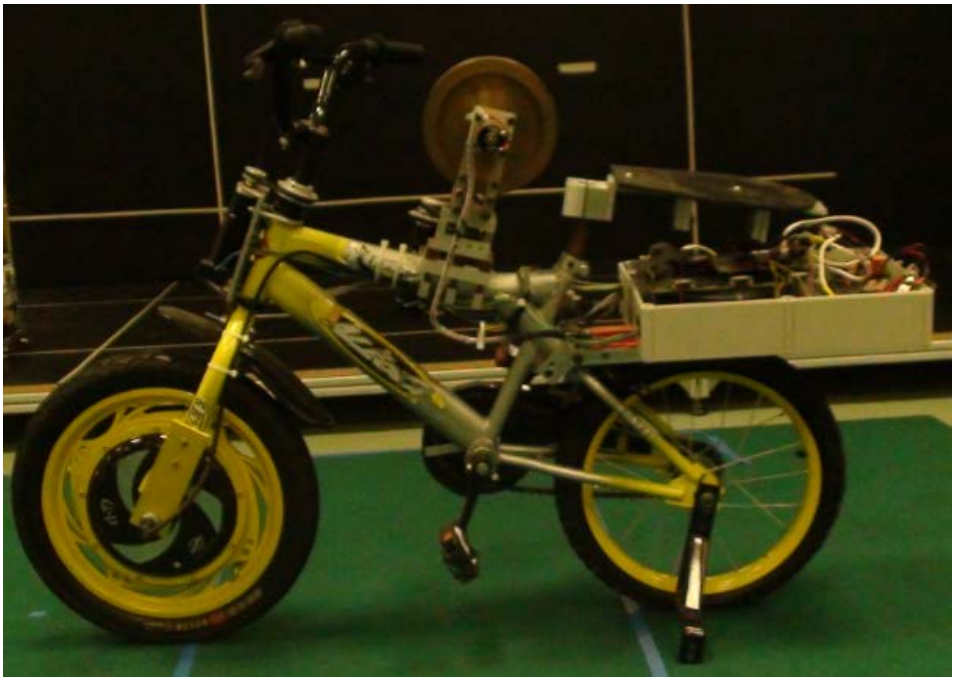

Figure 3.1: Bicycle with CMG.

3.2 Electronic - Embedded Controller

The embedded controller is a single-board reconfigurable IO (sbRIO) from National Instruments and it consist of a Freescale real-time processor, a Xilinx reconfigurable field-programmable gate array (FPGA), and 110 bidirectional digital

I/O lines along with RS232, Ethernet, and analogue I/O on a single board. All I/O is connected directly to the FPGA, providing low-level customization of timing and I/O signal processing. Both the real-time processor and FPGA is program through LabVIEW, a graphical programming environment developed by National Instruments. This setup provided seamless integration between the real-time processor and FPGA, and with high speed Ethernet communication; data such as response graph are easily generated in LabVIEW graphical interface.

3.3 Electronic – IMU Sensor

An Xsens MTi IMU (Figure 3.2) is used to detect the roll angle of the bicycle. The MTi is a miniature, gyro-enhanced Attitude and Heading Reference System (AHRS). Its internal low-power signal processor provides drift-free 3D orientation and calibrated 3D acceleration, a 3D rate of turn, and 3D earth-magnetic field data. The MTi is an excellent inertial measurement unit (IMU) for stabilization and control of cameras, robots, vehicles, and other stand-alone equipment. The MTi IMU communicates with the SbRIO via RS232 serial communication at a baud-rate of 115200bps.

Figure 3.2: XSens MTi IMU sensor.

3.4 DC Motor Amplifier Motor

The CMG's flywheel is driven by a Maxon DC motor and is powered by constant dc voltage. The CMG gimbal is driven by a Maxon brushless motor. Encoder signals are fed back to the FPGA of the SbRIO to be processed as angular positioning data.

3.5 Electrical Noise on Encoder Signals

The CMG's flywheel is driven by a Maxon DC motor and is powered by constant dc voltage. The CMG gimbal is driven by a Maxon brushless motor. Encoder signals are fed back to the FPGA of the SbRIO to be processed as angular positioning data. During initial testing of the CMG, it was found that the encoder attached to the

gimbal motor is susceptible to electrical noise. Encoder with differential encoder signals was used to resolve the issue. Differential wiring uses two wires per channel that are referenced to each other. The signals on these wires are always 180 electrical degrees out of phase, or exact opposites. This wiring is useful for higher noise immunity, at the expense of having more electrical connections. Differential wiring is often employed in “noisy” environments, when noise is picked up on the wiring is common mode rejected [21]. With reference to Figure 3-3, differential outputs provide two signal wires with exactly opposite signals on each wire. Any noise coupled into the system is common mode, or the same on both wires. Since a differential system is set up to look at only signals with exactly opposite voltage potentials, the noise component is rejected. On the receiving end, before channelling the signal to a counter, the inverted signal is inverted through an inverter and logically OR with the non-inverted signal. In a traditional approach in circuit design, additional circuit must be added to merge the differential encoder as shown in Figure 3.3. Taking advantage of FPGA on-board sbRIO, the circuit was built within the FPGA without any extra hardware. The result was a robust sensing system.

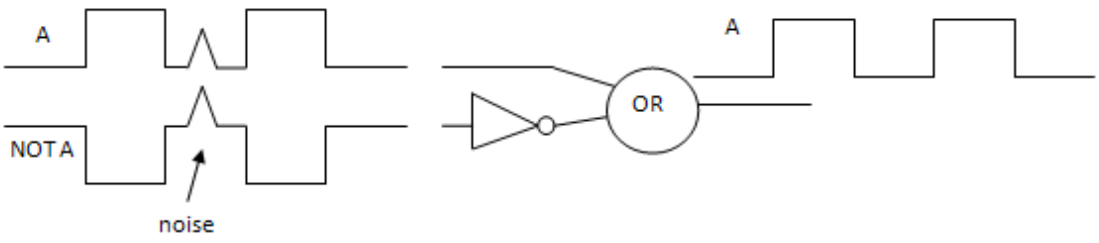

Figure 3.3: Circuit to eliminate distortion by complementary encoder signals (differential).

3.6 Integrated Electronic System

A PC is connected via the Ethernet to the SbRIO for software development and tuning gains. Critical encoder positioning data are sampled by the FPGA. Analogue output voltage for controlling the gimbal motor is sent from the FPGA. The closed-loop PID controller resides in the Freescale Power PC real-time processor. With LabVIEW Real-Time, PID gains were tuned on the fly via an Ethernet connection which greatly facilitated gain tuning as opposed to conventional programming.

Embedded controllers are usually programmed with the control algorithm with gains set constant at programming. If gains must be changed, which is done in most cases, the entire embedded controller with new gains must be reprogrammed, which is very inefficient and time-consuming.

In our approach, enabled with NI SbRIO and LabVIEW real-time, we are able to tune gains at run time, and, at the same time, view response graphs from the system. Critical parameters such as overshoot and system response can be easily analysed at run time. Figure 3.4 summarizes the electronic system.

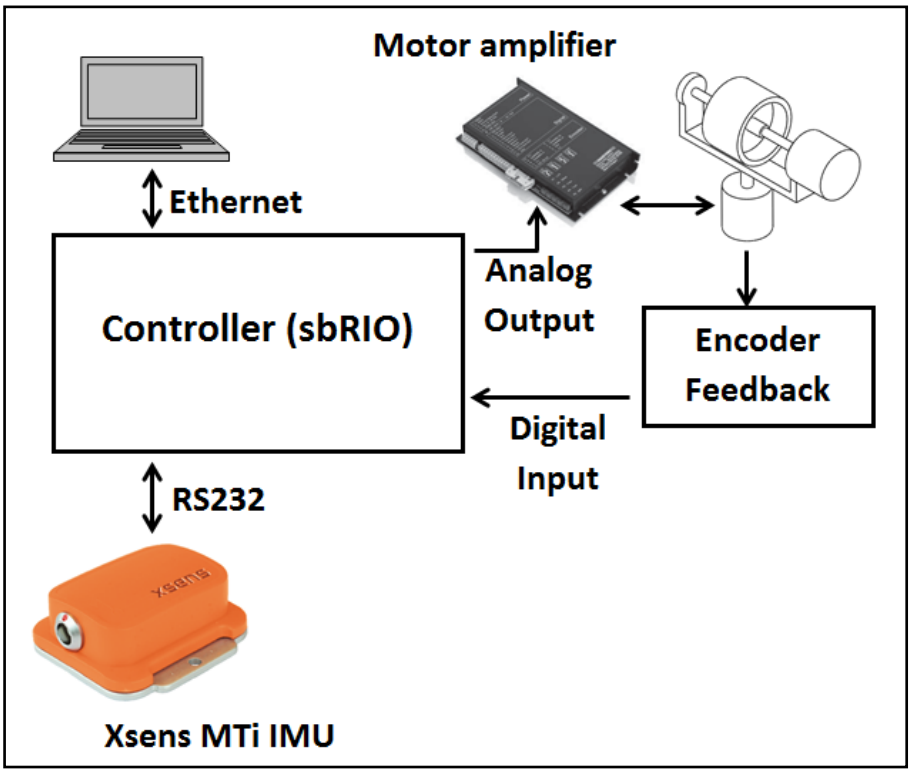

Figure 3.4: Components of electronic system.

3.7 Mechanical – Single Axis Control Moment Gyro (CMG)

Figure 3.5 shows the actual implementation of the single-axis CMG onto the frame of the kid size bicycle. The flywheel is driven by dc gyro motor and is allowed to run at its maximum angular velocity of 469 rad/s in order to generate the highest possible angular momentum. The gimbal axis is driven by a gimbal motor through belt drive and in this implementation, is a brushed dc motor.

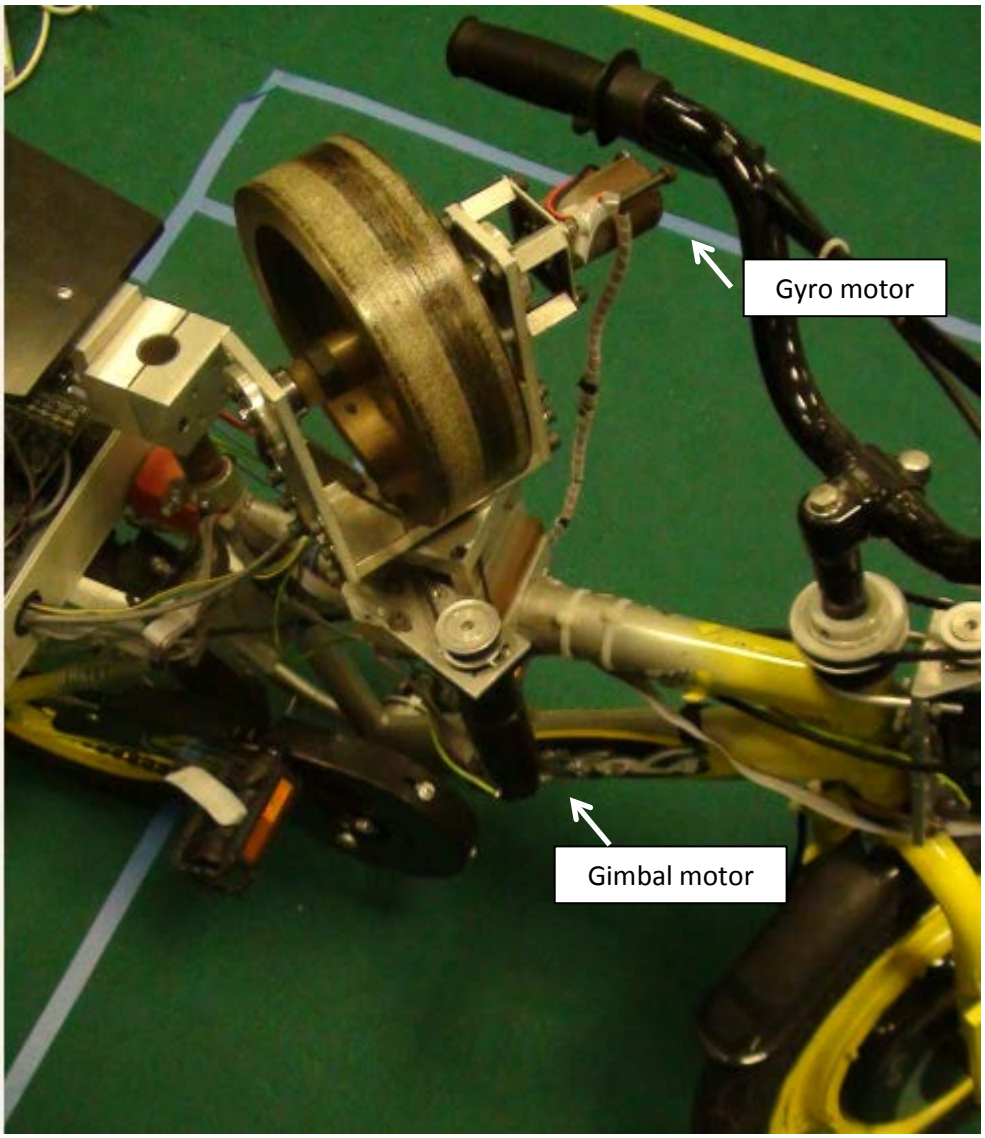

Figure 3.5: Control Moment Gyro (CMG) mounted on frame of bicycle.

Chapter 4. Real-Time Experiment

4.1 Stationary

Ziegler-Nichols rules for tuning PD gains were used to tune gains of the controller. Only proportional control action is used at first to attempt to balance the bicycle. K_p is increased from 0 until the bicycle oscillate about the vertical position. The D gain is slowly increased from zero until a suitable step response is achieved. Gains were fine-tuned to ensure that the system can withstand significant roll disturbance. The actual P-Gain used differs from those found in simulation and a P-Gain of 42 is used. Figure 4.1 shows the test setup whereby the bicycle is initially tilted at an angle of 11.6 deg and the controller commands the bicycle to take an upright position. Roll data is captured for different PD values.

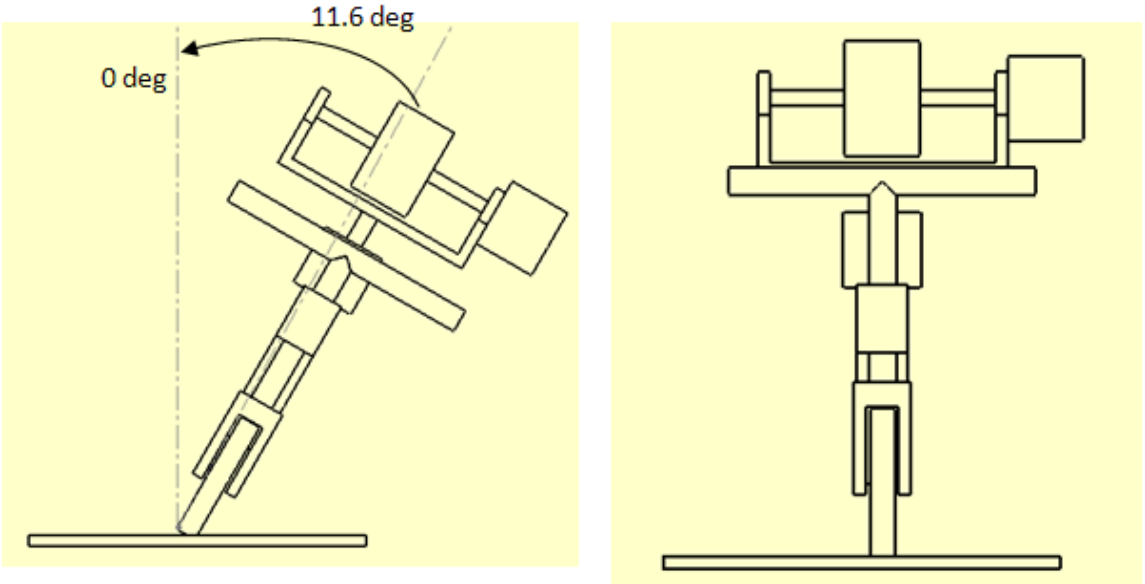

Figure 4.1: Experiment setup for step response.

Figure 4.2 to Figure 4.4 shows the result for varying the Proportional gain from 37 to 47 while keeping Derivative gain constant at 0.04. The result for peak time (T_{peak}), percent overshoot (%OS) and rise time (T_{rise}) are shown in Table 4.1. Peak time (T_{peak}) and Rise time (T_{rise}) decreases with increasing P-Gain, % overshoot increases with P-Gain. The proportional term produces an output value that is proportional to the current error value [22]. The proportional response is adjusted by multiplying the error by a constant K_p. A small gain results in a small output response to large input error, and a less responsive or less sensitive controller. A high proportional gain will result in a large change in the output for a given change in the error. If the proportional gain is too large, the system can become unstable.

Table 4.1: Key parameters.

P=37, D=0.04	**T_{peak} (s)**	1.164
	%OS	5.4
	T_{rise} (s)	0.29
	Peak-to-Peak Oscillation (deg)	3
P=42, D=0.04	**T_{peak} (s)**	1.086
	%OS	7.4
	T_{rise} (s)	0.178
	Peak-to-Peak Oscillation (deg)	2
P=47, D=0.04	**T_{peak} (s)**	0.726
	%OS	12.7
	T_{rise} (s)	0.146
	Peak-to-Peak Oscillation (deg)	2

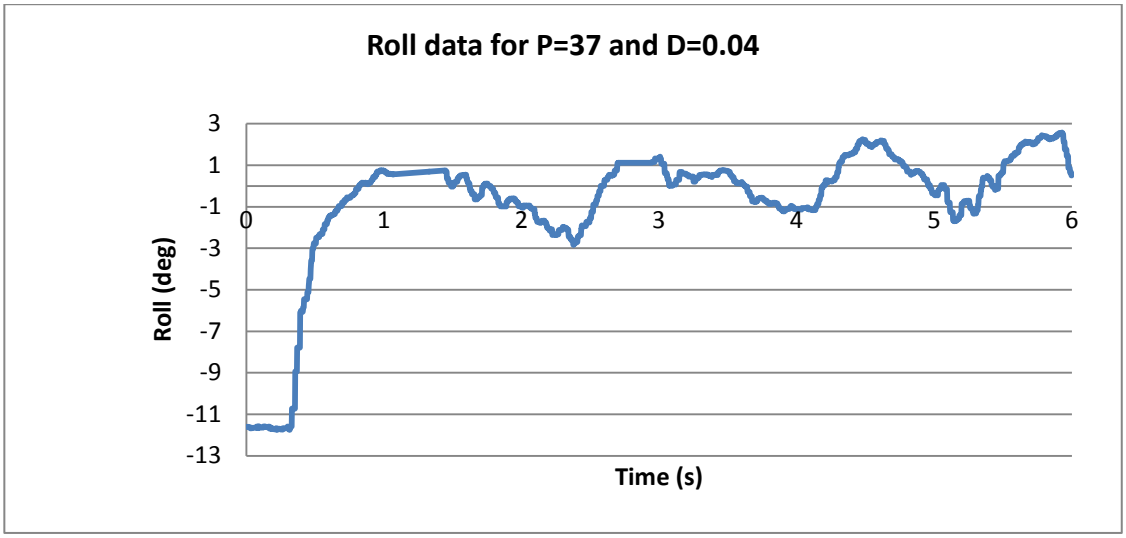

Figure 4.2: Roll data for P=37 and D=0.04.

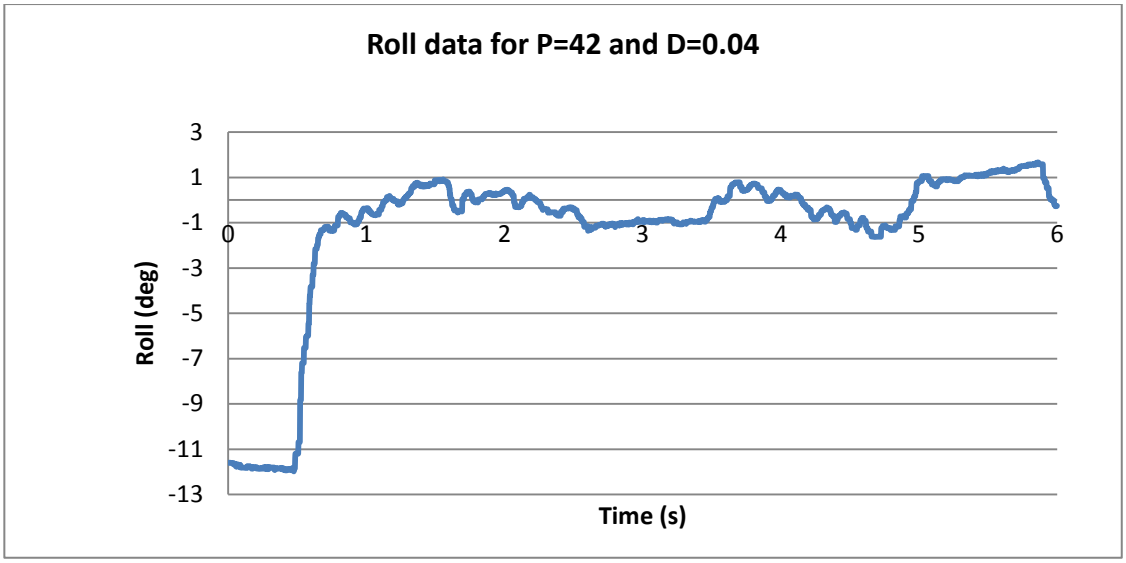

Figure 4.3: Roll data for P=42 and D=0.04.

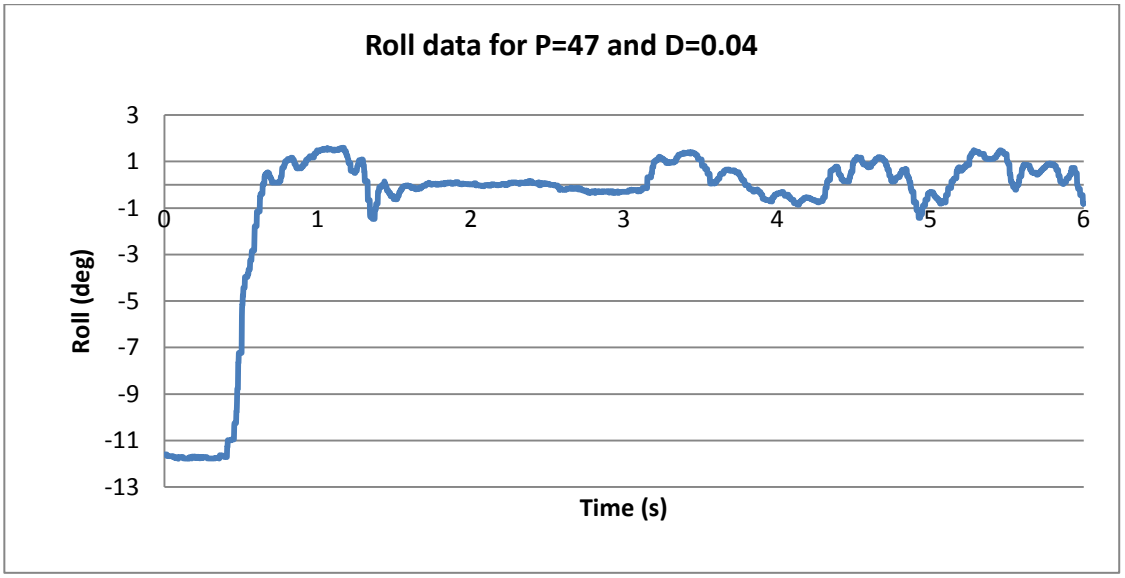

Figure 4.4: Roll data for P=47 and D=0.04.

P-gain is kept constant while D-gain is varied. The various roll response from varying D gain are shown in Figure 4.5 to Figure 4.7.

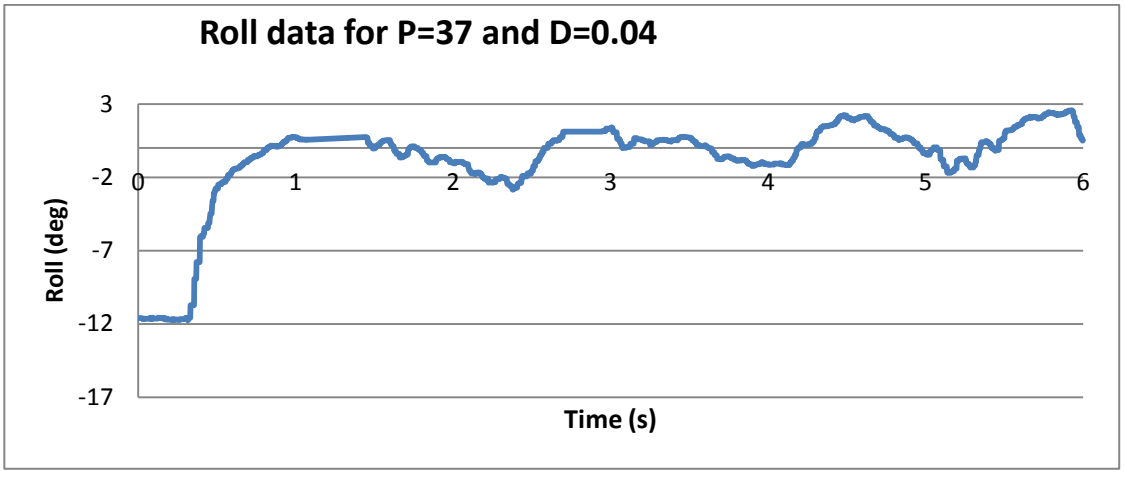

Figure 4.5: Roll data for P=37 and D=0.04.

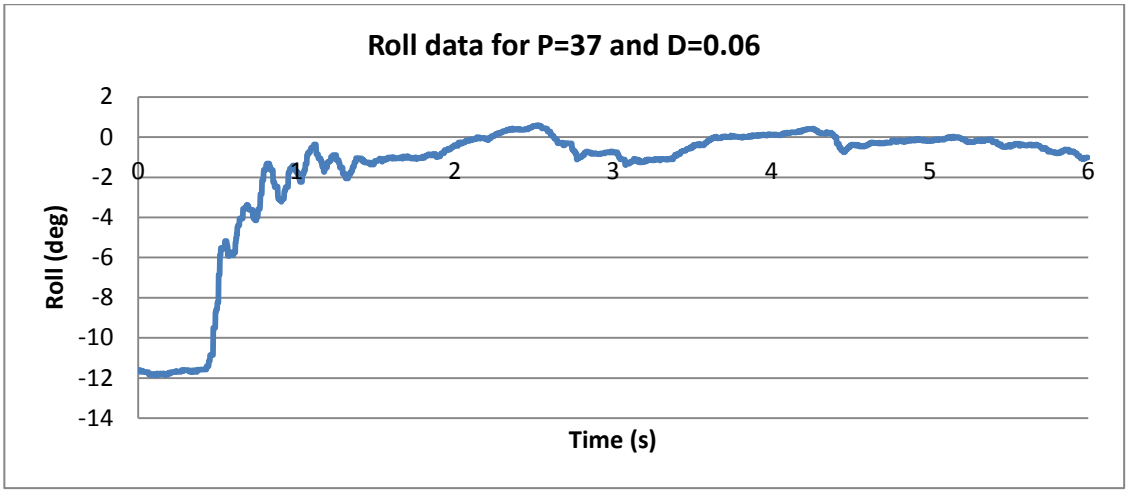

Figure 4.6: Roll data for P=37 and D=0.06.

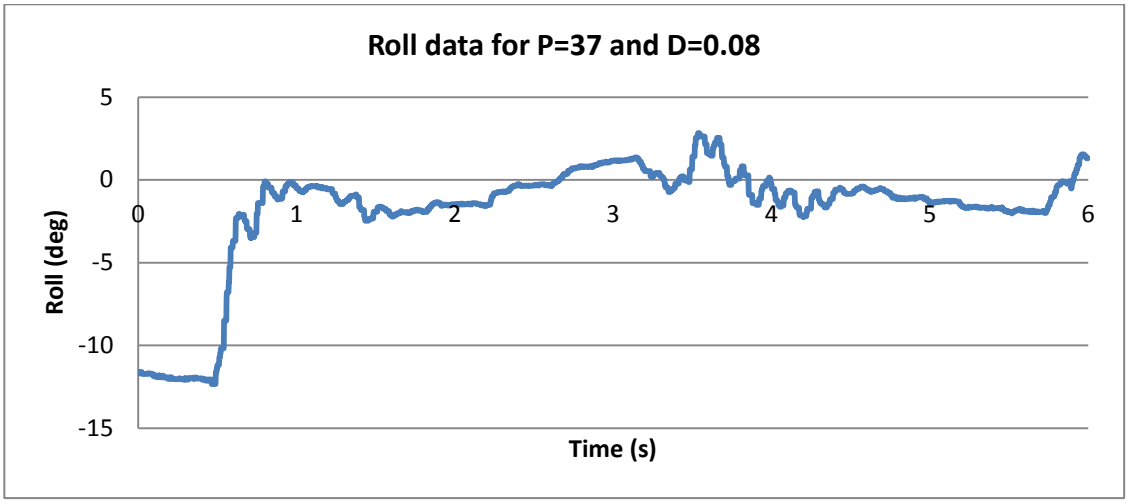

Figure 4.7: Roll data for P=37 and D=0.08.

Table 4-2 summarizes the peak-to-peak oscillation of roll data. Derivative term has effect of adding damping to the system. As the derivative term dampens the controller output, T_{peak} increases with D-gain. Peak-to-peak oscillation was the smallest at a D-gain of 0.06. Beyond a D-gain of 0.08, the peak-to-peak oscillation will increase and the bicycle would be unstable. Based on the data, D-gain should not exceed 0.06.

Table 4.2: Results of critical parameters.

P=37, D=0.04	**T_{peak} (s)**	1.1
	%OS	7.4
	T_{rise} (s)	0.18
	Peak-to-Peak Oscillation (deg)	4
P=37, D=0.06	**T_{peak} (s)**	2.09
	%OS	4.02
	T_{rise} (s)	0.67
	Peak-to-Peak Oscillation (deg)	2
P=37, D=0.08	**T_{peak} (s)**	2.68
	%OS	9.83
	T_{rise} (s)	0.45
	Peak-to-Peak Oscillation (deg)	5

As evident from Table 4.2, increasing D-Gain slows the rate of change of the controller. Derivative control will reduce the magnitude of the overshoot produced and improve the system stability [21]. However, the derivative term slows the transient response of the controller. Also, differentiation of signal amplifies noise and will make the controller highly sensitive to noise in the error term, and can cause the bicycle to become oscillatory due to the effect of noise when the noise and the derivate gain are sufficiently large as can be seen in Figure 4.7 when the D-Gain is 0.08.

The final gains to be used for balancing the bicycle have a P gain of 47 and D gain of 0.04. This selection is a trade-off between performance and stability. As can be

seen from Figure 4.5, these gains produce a relativity fast response and acceptable steady state oscillation of within +/- 1.5 deg.

4.2 Translational Motion of Bicycle while Balancing

This section describe the basic motion such as moving forward, reverse, turning left and right of the bicycle. The front wheel of the bicycle is a brushless hub-less motor that is widely used in commercial electrical bicycles. A brushless motor driver from Maxon was used to drive the front wheel. The handle bar of the bicycle is coupled via a belt drive to a brushed motor as shown in Figure 4.8. Both the front wheel and steering angle of the handle bar can be remotely controlled.

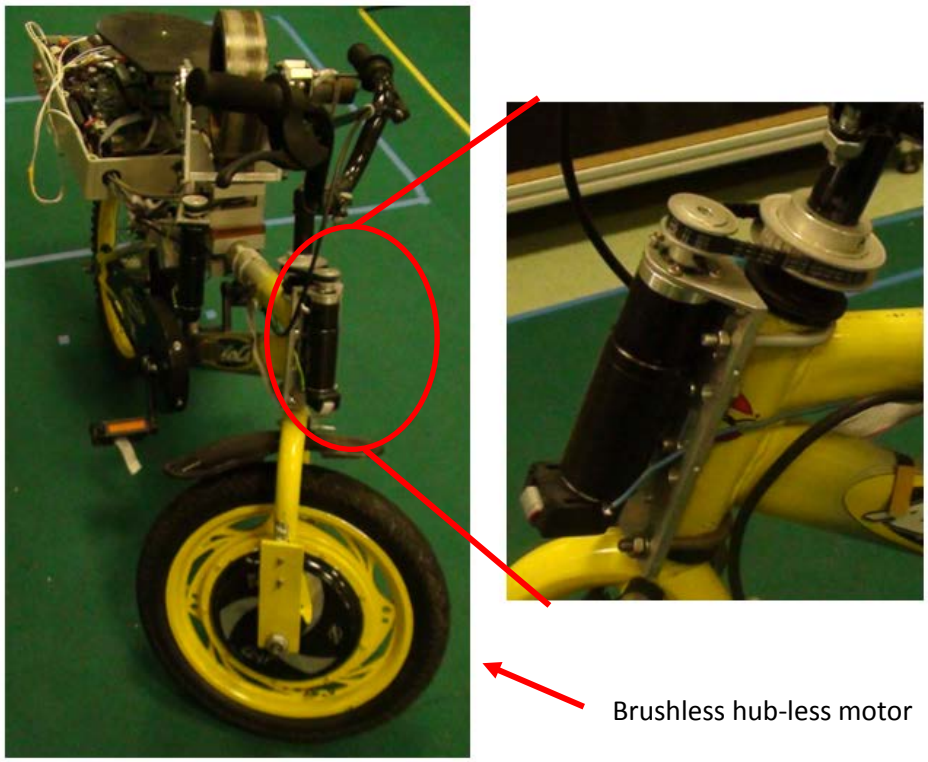

Figure 4.8: Powered front wheel and steering.

4.3 Forward

The bicycle had no technical problems while moving forward and reversesing. This is due to the fact that the COG of the bicycle remains unchanged. Except for the initial move off from a stationary position, the bicycle experienced a “jerk” motion. During initial testing, the bicycle had difficulties when turning left or right. The COG of the bicycle changes as the handle bar angles deviates from the position that makes the bicycle forward and reverse. Figure 4.9 shows the roll angle when the bicycle starts off with stationary balancing, moving forward and followed by a 10 degree left turn on the handle bar. . The roll is acceptable except for the initial “jerk” while the powered front wheel overcomes its inertial from stationary to moving forward and after which the performance is comparable to while the bicycle is stationary.

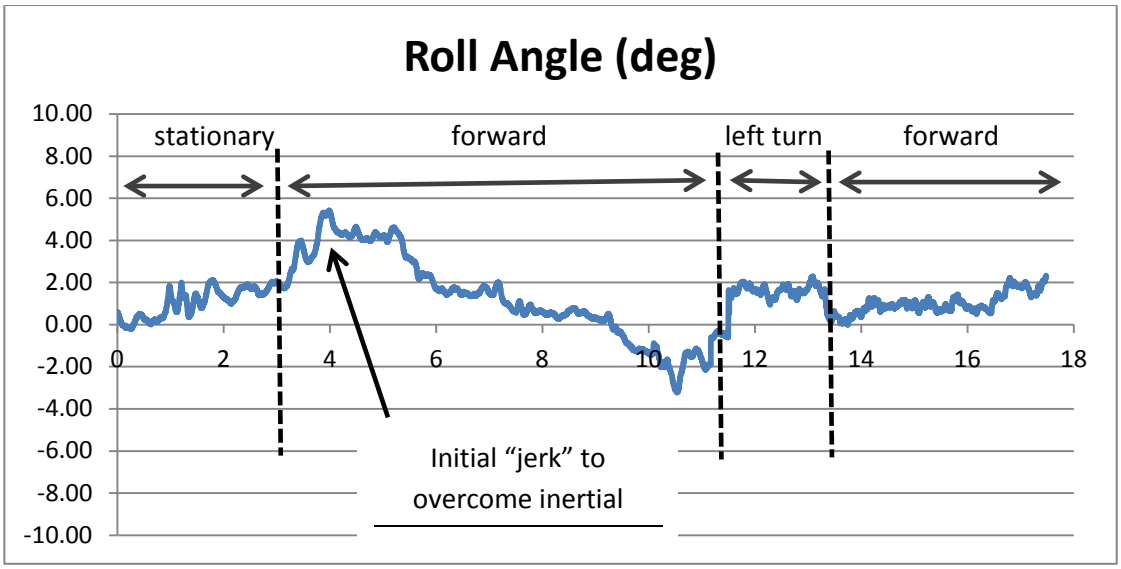

Figure 4.9: Roll data of bicycle in motion.

4.4 Turning

With reference to Figure 4.10, α denotes the handle bar angle while (following earlier definition) δ denotes the angle of CMG with respect to the frame of the bicycle frame. It was observed that while balancing the bicycle and keeping the bicycle stationary, varying α will cause δ to change as shown in Figure 4.11, because of the change in cg of the bicycle.

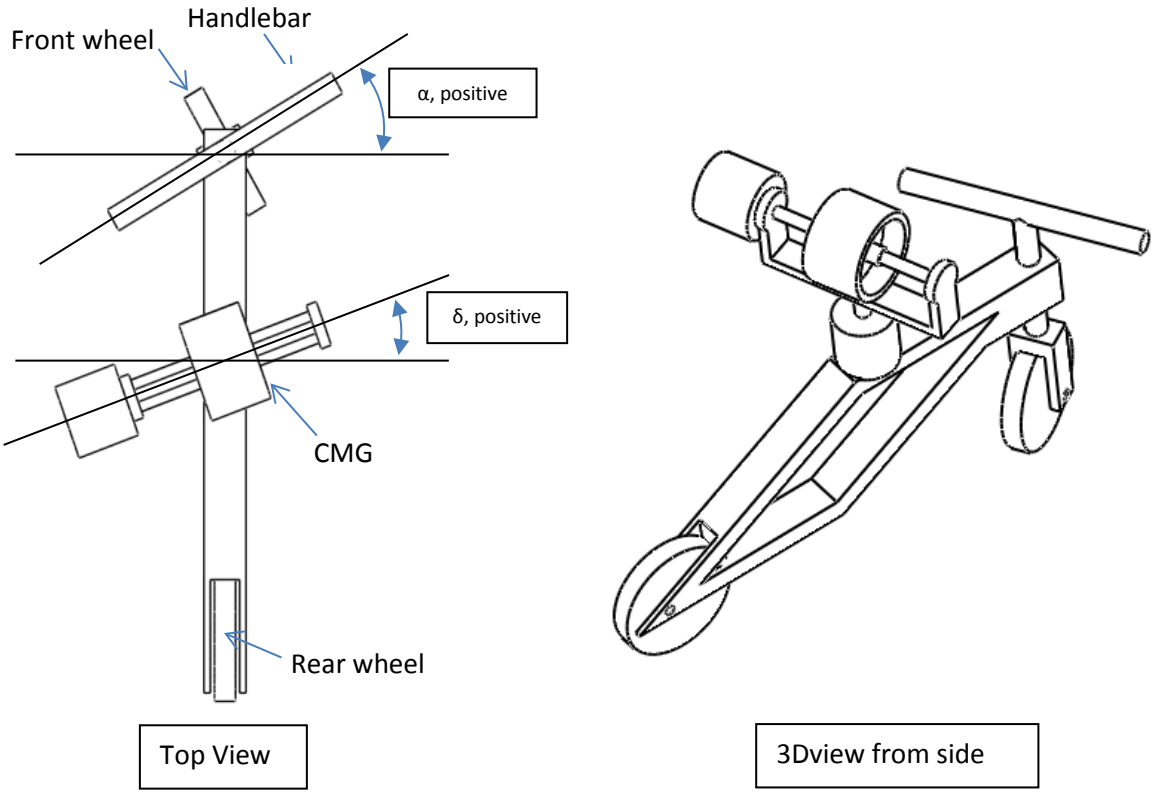

Figure 4.10: Definition of angle α and δ with respect to frame of bicycle.

Angle δ is affected by angle α; gyroscope is most effective around the zero precession angle and ideally angle δ should be independent of angle α or any changes to the handle bar should not affect the angle of CMG with respect to the frame of the bicycle frame. The working range of δ is about +/- 45 degree; beyond this range the

torque generated is unable to restore the bicycle to an upright position. Experiments were carried out to characterise the relationship between the handle bar angle, α and the orientation of the CMG, δ. Figure 4.12 is the experiment data to correlate handle bar angle, α to CMG angle, δ.

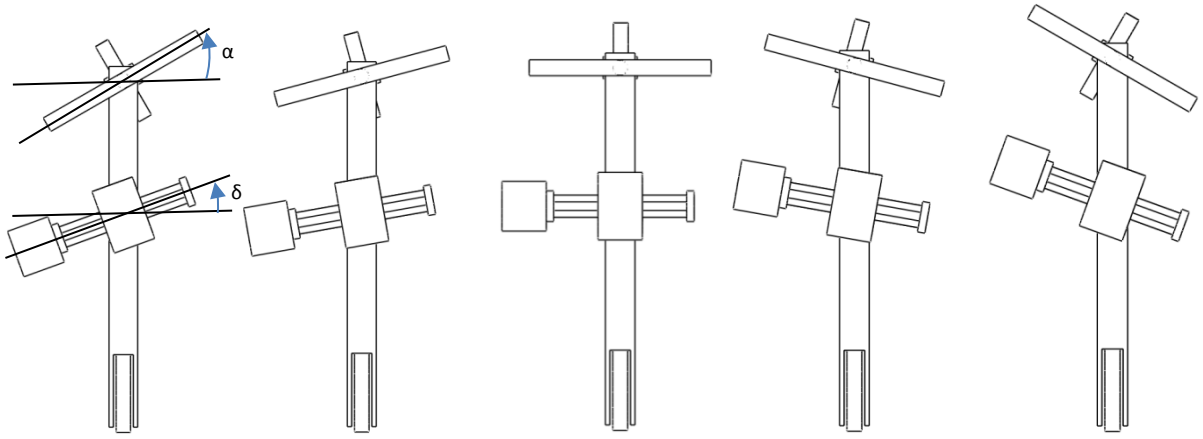

Figure 4.11: Effect of angle α on angle δ.

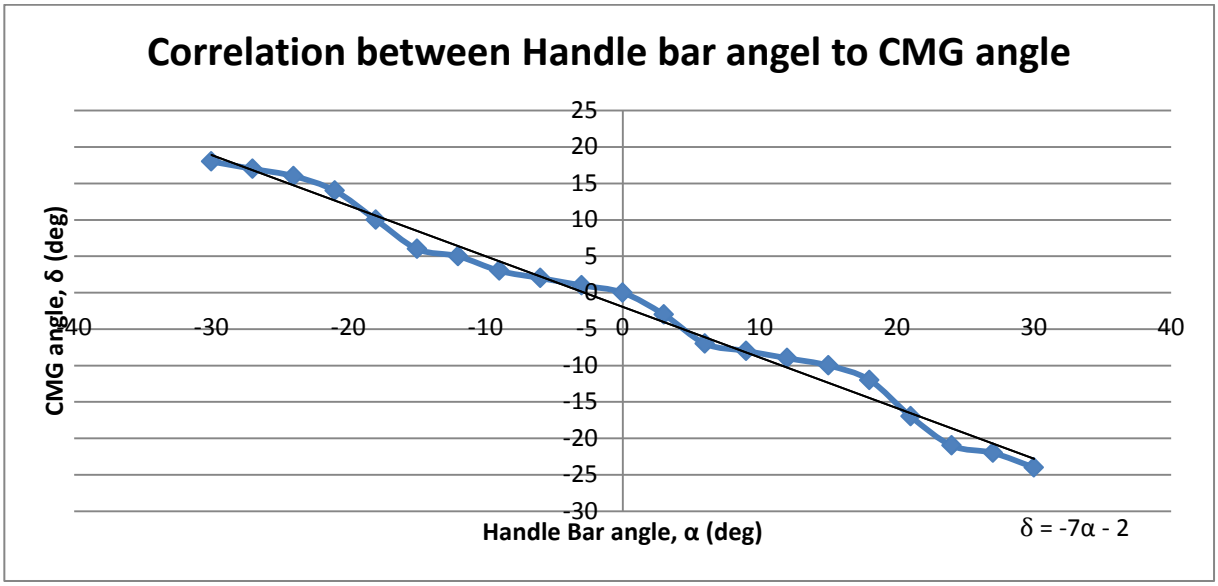

Figure 4.12: Correlation of angle α to angle δ.

The linear best fit equation

$$\delta = -7\alpha - 2 \tag{4.1}$$

would be used to create the required offset to be applied to the setpoint of the CMG position. Whenever the handlebar rotates, the controller will read in the handlebar angle, α and apply an appropriate offset generated by equation (4.1) to the CMG angle, δ. Figure 4.13 illustrate how the offset is applied to the control system. The offset compensation can easily be added to the controller without affecting the PD controller. Figure 4.9 shows the roll data of the bicycle while it was executing a left turn of 10 degree. During a turn of 10 degree to the left, the bicycle was tilted at positive 2 degree due to the centrifugal force experienced by the bicycle while maneuvering the turn. [23] is a video presentation of the bicycle in various motion such as forward, turning left and right.

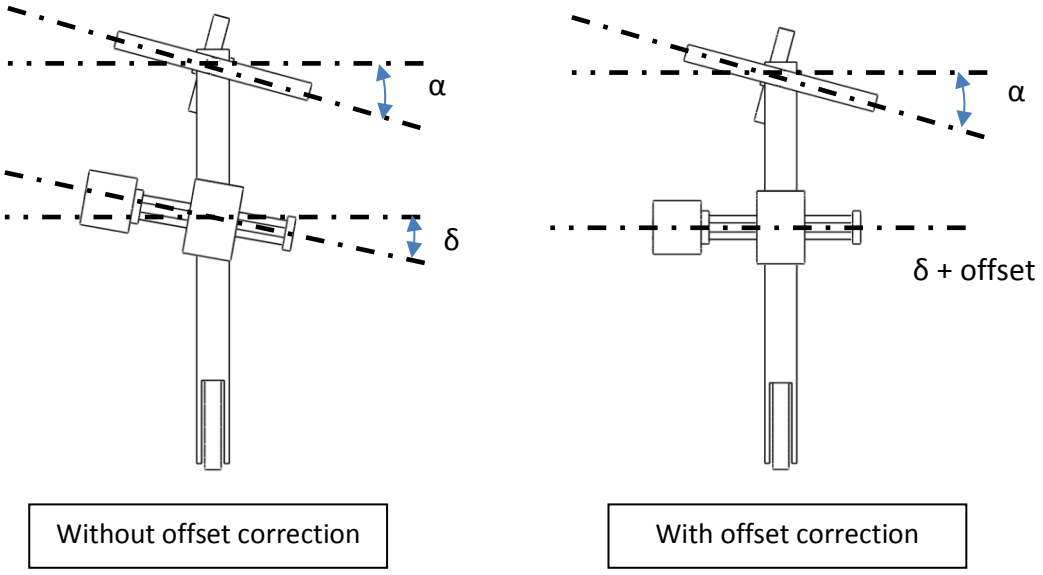

Figure 4.13: Implementation of offset to correct angle δ.

Chapter 5. Conclusions

5.1 Summary

This thesis presents work on the use of a Control Moment Gyro (CMG) and a PD controller to balance a bicycle. The CMG was used as a momentum exchange actuator to balance the bicycle. The CMG is an effective torque amplification device and has a short response time.

A state space model of the bicycle with the CMG and a closed-loop controller was created in the control design assistant developed by National Instruments. Simulations were used to determine the performance of the controller and to find initial gains to be used in a real-time system for deployment. Simulation exercises showed that a PD controller is adequate for balancing the bicycle. A PID decreases the phase margin dramatically and the system becomes unstable and unable to balance the bicycle.

The real-time controller was implemented on a sbRIO and programmed in LabVIEW. This approach dramatically shortened development time for the PD controller, and was made possible with intuitive graphical LabVIEW programming, enabling data to be easily viewed and manipulated at run-time. With the possibilities of FPGA programming within LabVIEW, this has further enhanced the capability of

LabVIEW for embedded applications. Filters can, for example, be easily added at no extra hardware cost.

5.2 Future Works

The current system is not adaptive and cannot react to changes such as increase in payload that will subsequently affect the COG. The full potential of the sbRIO is also not realised, a lot more function can be added into sbRIO. Recent software development from National Instruments allows system identification to be implemented within the sbRIO at runtime. With system identification and balancing algorithm running at the same time, the system can be adaptive; reacts automatically to changes in payload. The project can be further developed into an autonomous self-balancing bicycle by incorporating for example, a LIDAR (Light Detection and Ranging) sensor to sense the environment [24].

5.3 Achievements

The self-balancing robot bicycle had won several awards locally and internationally, two conference paper and one journal was published.

- Won the second prize at the Open Category of Singapore Robotics Games 2011 [25].
- Won the second prize at the Category D or Open Category of the Amazing Science X Challenge (ASXC) 2011, Singapore [26].

- Won the Best Innovation in Robotics award of the National Instruments (NI) Asean Graphical System Design Awards 2011, International [27].
- Published a conference paper entitled "Design and Development of a Self-Balancing Bicycle Robot" in Fourth Asia International Symposium on Mechatronics (AISM 2010)
- Published a journal paper entitled "Gyroscopic Stabilization of a Self-Balancing Robot Bicycle" in the International Journal of Automation Technology (IJAT) 2011 Volume 5 No. 6 issue [28].
- Published a conference paper "Gyroscopic Stabilization of a Kid-Size Bicycle" in the Fifth IEEE International Conference on Cybernetics and Intelligent Systems and the Fifth IEEE Conference on Robotics, Automation and Mechatronics (CIS and RAM) 2011 [29].

References

[1] D. Herlihy, Bicycle: The History, New Haven, CT: Yale Univ. Press, 2004.

[2] Proceeding International Cycling Hostory Conference, Freehold, NJ, July 29 Aug 1, 2009.

[3] K. Astrom, R. Klein, and A. Lennartsson, "Bicycle dynamics and control," IEEE Control Syst. Mag., vol. 25, no. 4, pp. 26–47, 2005.

[4] V. Cerone, D. Andreo, M. Larsson, D. Regruto, "Stabilization of a Riderless Bicycle A Linear-Parameter-Varying Approach," IEEE Control Syst. Mag., vol. 30, no. 5 pp. 23–32, 2010.

[5] H. Kurokawa, "A Geometric Study of Single Gimbal Control Moment Gyros." Agency of Industrial Technology and Science, Ministry of International Trade and Industry, Japan, Report of Mechanical Engineering Laboratory, 1997.

[6] K. Yamafuji, "Useful Robots and Hopeful Robots", Fuji Technology Press, 2011.

[7] Girouart, B., Sebbag, I., and Lachiver, J., "Performance of the Pleiadee-HR Agile Attitude Control System," Proceedings of ESA International Conference

on Spacecraft Guidance, Navigation and Control Systems, ESA, Noordwijk, The Netherlands, 2002, pp. 497-500.

[8] Beznos AV, Formalsky AM, Gurfinkel EV, Jicharev DN, Lensky AV, Savitsky K V, et al. “Control of autonomous motion of two-wheel bicycle with gyroscopic stabilization.” In:Proceedings of the IEEE international conference on robotics and automation, 1998, p. 2670-5.

[9] Lee S, Ham W. “Self-stabilizing strategy in tracking control of unmanned electric bicycle with mass balance.” IEEE international conference on intelligent robots and systems, 2002, p. 2200-5.

[10] Tanaka Y, Murakami T. “Self Sustaining Bicycle Robot with Steering Controller,” Proceedings of international workshop on advanced motion control, 2004, p. 193-197.

[11] The Murata Boy Website.[Online]. Available from http://www.murataboy.com/en/

[12] Gallaspy JM. “Gyroscopic stabilization of an unmanned bicycle, M.S. Thesis,” Auburn University, 1999.

[13] M. Romano, B. N. Agrawal, “Attitude Dynamics/Control of Dual-Body Spacecraft with Variable-Speed Control Moment Gyros,” Journal of Guidance, Control and Dynamics, vol. 27,no. 4, pp. 513-525, 2004.

[14] X. Roser, M. Sghedoni, “Control Moment Gyroscopes (CMG's) and their Application in Future Scientific Missions,” Spacecraft Guidance, Navigation and Control Systems, Proceedings of the 3rd ESA International Conference, 1996, pp. 523-528

[15] C. Clark, K. Worrall, E. Yavuzoglu, “A Control Moment Gyro for Dynamic Attitude Control of Small Satellites.” Conference on Small Satellites, 24th Annual AIAA/USU

[16] Youtube video to illustrate how gyroscopic torque is harnessed to balance a bicycle, available from http://www.youtube.com/watch?v=GtpvieNuqi0&feature=plcp

[17] BUI, T.T. and Parnichkun, M. Balancing of Bicyrobo by particle swarm optimisation based structure-specified mixed H2/H∞ control. International Journal of Advanced Robotic Systems, 2008, 5(4), 395-402.

[18] Nise N. S. Control Systems Engineering 2nd Edition, pp. 160-195, Addison-Wesley, 1995

[19] C. Dorf, H. Bishop, “Modern Control System,” 12th Edition, pp. 653-661, Prentice Hall, 2011.

[20] O. Katsuhiko, “Modern Control Engineering Fourth Edition,” pp. 682-683, Prentice Hall, 2003

[21] John R. Barnes, “Robust Electronic Design Reference Book,” vol. 1, ch. 22, pp. 15, Kluwar Academic Publisher, 2004.

[22] C. Dorf, H. Bishop, "Modern Control System," 12th Edition, pp. 480-491, Prentice Hall, 2011.

[23] Youtube video to show CMG-controlled self-balancing bicycle in motion, available from http://www.youtube.com/watch?v=HeWjGKFD59g&feature=youtu.be

[24] Conference articles:
I. Puente, H. Gonzalez-Jorge, P. Arios, J. Armesto, lan-Based Mobile Laser Scanning System, a review. International Society for Photogrammetry and Remote Sensing (ISPRS) Workshop for Laser Scanning, 2011.

[25] Official results of Singapore Robotics Games 2011, first runner-up of Open-Category, Acrobat Bobby, available from http://guppy.mpe.nus.edu.sg/srg/srg11/SRG2011OfficialResults.pdf

[26] Official results of Amazing Science-X Challenge (ASXC) 2011, first runner-up of Category D, Self-Balancing Bicycle, available from https://www.dso.org.sg/news_details.aspx?news_sid=20111010465464102113

[27] Winner of Best Innovation in Robotics of National Instruments ASEAN Graphical System Design Achievement Awards 2011 [online]. Available at http://singapore.ni.com/gsdawards/2011-winners

[28] P. Y. Lam, T. K. Sin, "Gyroscopic Stabilization of a Self-Balancing Robot Bicycle." IJAT publication, Vol 5, No 6, Nov 2011

[29] Pom Yuan Lam, Gyroscopic Stabiliztion of a Kid-Size Bicycle. Cybernetics and Intelligent System (CIS), 201 IEEE 5th International Conference. pp. 247-252, 2011.